

THESIS FOR THE DEGREE OF DOCTOR OF PHILOSOPHY

Characterization and Design  
Requirements for Antennas in the  
Near-field and the Random-LOS  
Propagation Environment

AIDIN RAZAVI



**CHALMERS**

Department of Signals and Systems  
CHALMERS UNIVERSITY OF TECHNOLOGY

Göteborg, Sweden 2016

**Characterization and Design Requirements for Antennas in the  
Near-field and the Random-LOS Propagation Environment**

AIDIN RAZAVI

ISBN 978-91-7597-494-1

© AIDIN RAZAVI, 2016.

Doktorsavhandlingar vid Chalmers tekniska högskola

Ny serie nr 4175

ISSN 0346-718X

Department of Signals and Systems

Antenna Systems Division

CHALMERS UNIVERSITY OF TECHNOLOGY

SE-412 96 Göteborg

Sweden

Telephone: +46 (0)31 – 772 1000

Email: [aidin.razavi@chalmers.se](mailto:aidin.razavi@chalmers.se)

[aidin.razavi@tgeik.com](mailto:aidin.razavi@tgeik.com)

Typeset by the author using L<sup>A</sup>T<sub>E</sub>X.

Chalmers Reproservice  
Göteborg, Sweden 2016

To *Baba, Maman, Azin*  
and my beloved  
*Maryam*



# Abstract

The choice of antenna for a particular application depends on the requirements imposed by that application. These include the field region (i.e., near-field or far-field), polarization, radiation pattern, radiation efficiency, system throughput, etc. Accordingly, during an antenna's design process, different characteristics and characterization methods have to be taken into account. The present thesis focuses on two different aspects of antenna characterization and design: The first concerns antennas in near-field applications dealing with lossy materials. The second is on the Over-The-Air (OTA) measurements of wireless devices and the Random-Line-Of-Sight (Random-LOS) environment.

The characterization, design criteria, and fundamental limitations of antennas in the near-field, especially in lossy media, have not been addressed as thoroughly as in the far-field. We introduce 3dB near-field beam radius ( $r_{3\text{dB}}$ ) as a measure to characterize the near-field focus of antenna apertures in the presence of loss in the medium. The  $r_{3\text{dB}}$  is then used to estimate the optimal size of uniform apertures that maximizes the scattered power from foreign objects in near-field sensing applications in lossy media. In addition, we present a generic numerical method for determining the optimal aperture field distribution that maximizes the near-field power transfer through lossy media, given the aperture size. Maximizing the power transfer is shown to result in increased sensitivity to the presence of foreign objects in lossy media. The method is applied to both homogeneous and planar multi-layered media and can be extended to any non-homogeneous media, given that the Green's function is known for the medium.

OTA testing of wireless systems is performed in an emulated propagation environment with the objective to evaluate the system performance in a reliable, repeatable and controllable way. A complete understanding of the propagation channel and the choice of the most representative model is still a challenge, let alone emulating it in an OTA measurement setup. Instead, we can gain valuable insight into the performance of a wireless system by investigating it in two edge environments, i.e., the Rich Isotropic Multipath (RIMP) and Line-of-Sight (LOS) environments. LOS is especially relevant

## ABSTRACT

in vehicular wireless communications in suburban and rural environments. The same is true in 5G systems where mm-wave radio links, small cells, and advanced beam forming are foreseen. However, such links undergo slow fading due to the random orientations of the user terminals or vehicles, therefore it is important to consider this in the propagation environment that is used. The Random-LOS environment has been introduced to take this effect into account.

Regarding the Random-LOS environment, we first investigate the design requirements for polarization-MIMO antennas to ensure good performance in the Random-LOS environment. We define two polarization-deficiencies in the radiation pattern of dual-polarized antennas and show that in Random-LOS these two are the main contributing parameters to sub-optimal performance of polarization-MIMO systems in terms of MIMO efficiency. The characterization method is used to study the performance of a novel dual-polarized MIMO antenna for micro base-stations. Also, a measurement setup and characterization method for OTA Random-LOS measurement of automotive wireless systems is proposed. The test setup is characterized in terms of the performance of an ideal probe antenna and an ideal receiver in the test zone of the measurement chamber. Finally, we provide a “back-of-the-envelope” investigation of the prevalence of RIMP or Random-LOS propagation in scattering environment as a function of frequency from 500 MHz to 100 GHz.

**Keywords:** Antenna measurements, antenna characterization, near-field antennas, near-field focusing, OTA, Random-LOS, MIMO, polarization-MIMO.

# Acknowledgment

After months of writing this thesis, this is the last and also the hardest part that I'm writing. This journey of five years, has been rich with valuable experiences and unforgettable memories. I have enjoyed the help and company of many wonderful people and I'm not sure I will be able to properly thank them all.

First and foremost, I wish to express my deepest gratitude to Professor Per-Simon Kildal for his guidance and encouragement, and for creating a great research environment in the Antenna systems division. His sudden departure caused us deep sorrow. His vision and enthusiasm were the driving forces behind the Random-LOS research and it saddens me that he's not with us to witness it flourish in the coming years. If I've learned one lesson from him, that is to fight for what you believe in.

I would like to thank my supervisor Associate Professor Jian Yang, for giving me the great opportunity to join the antenna group and for his support and trust during these years. Many thanks to my co-supervisors Assistant Professors Rob Maaskant and Andrés Alayón Glazunov for the interest, attention and time they have put in this work. Furthermore, I wish to express my gratitude to Professor Mats Viberg for examining this thesis and for his warm and encouraging attitude.

Thanks to all former and current colleagues in the Signals and Systems department and the Antenna systems division, for contributing to a nice and enjoyable work environment. I have been fortunate to work with all of you in such a friendly and multi-cultural place. I would like to particularly thank my dear friends Astrid, Abbas, Carlo, Madeleine, Pegah, Sadegh and Samar. We have kept each other company during both happy times and sad times, and that is what friends are for. Special thanks to Carlo and Madeleine for proofreading this thesis.

I have been lucky for being surrounded with many great Iranian friends: Azita, Bahram, Behrooz, Mitra, Mona, Negar, Roozbeh. Thank you for reminding me of home. Special thanks to Ali and Sahar, for their kind friendship and for making it much easier for us to settle down in a new country.

## ACKNOWLEDGMENT

I would like to express my deepest gratitude to my father for continuously encouraging my curiosity, my mother whose endless patience is an inspiration to me, and my sister whose artistic and daring spirit I admire. Special thanks to my in-laws for their never-ending support and kind hearts.

To my dearest Maryam, you are a constant source of energy to me. I can only hope to be able to express how blessed I am to have you beside me. Thanks for your lovely company through life's endeavor.

*Aidin Razavi*  
*November, 2016*

# List of Abbreviations

5G	5th generation mobile networks
AoA	Angle of Arrival
AUT	Antenna Under Test
AWGN	Additive White Gaussian Noise
CDF	Cumulative Distribution Function
CSI	Channel State Information
DC	Direct Current
EGC	Equal-Gain Combining
EM	Electromagnetic
EMC	Electromagnetic Compatibility
FM	Frequency Modulation
IEEE	Institute of Electrical and Electronics Engineers
LOS	Line of Sight
MIMO	Multiple-Input Multiple-Output
MoM	Method of Moments
MRC	Maximal Ratio Combining
OFDM	Orthogonal Frequency-Division Multiplexing
OTA	Over The Air
PEC	Perfect Electric Conductor
PoD	Probability of Detection
Random-LOS	Random Line of Sight
RIMP	Rich Isotropic Multipath
SC	Selection Combining
SIMO	Single-Input Multiple-Output
SISO	Single-Input Single-Output
SNR	Signal-to-Noise Ratio
SSC	Switch and Stay Combining
SVD	Singular Value Decomposition
ZF	Zero Forcing



# List of Publications

This thesis is based on the work contained in the following appended papers:

## Paper 1

**A. Razavi**, and J. Yang, “Optimal Size of Uniform Aperture for Near-field Penetration Through Lossy Medium”, *Microwave and Optical Technology Letters*, Vol. 56, No. 10, pp. 2301–2304, October 2014.

## Paper 2

**A. Razavi**, R. Maaskant, J. Yang, and M. Viberg, “Maximum Aperture Power Transmission in Lossy Homogeneous Matters”, *IEEE Antennas and Wireless Propagation Letters*, Vol. 14, pp. 175-178, 2015.

## Paper 3

**A. Razavi**, R. Maaskant, J. Yang, Z. Šipuš, and M. Viberg, “Optimal Aperture Distribution for Maximum Power Transfer in Planar Lossy Multilayered Matters”, in *Proceedings of the 9<sup>th</sup> European Conference on Antennas and Propagation (EuCAP 2015)*, Lisbon, Portugal, April 2015.

## Paper 4

**A. Razavi**, A. Alayón Glazunov, P.-S. Kildal, and J. Yang, “Characterizing Polarization-MIMO Antennas in Random-LOS Propagation Channels”, *IEEE Access*, Manuscript accepted for publication, 2016.

## Paper 5

**A. Razavi** and A. Alayón Glazunov, “Probability of Detection Functions of Polarization-MIMO Systems in Random-LOS”, To be submitted.

## Paper 6

**A. Razavi**, W. Yu, J. Yang, and A. Alayón Glazunov, “Design of a Planar Eleven Antenna for Optimal Probability of Detection as a Wideband MIMO Micro-base Station Antenna”, Submitted to *IEEE Transactions on Antennas and Propagation*.

**Paper 7**

**A. Razavi**, A. Alayón Glazunov, S. Mansouri Moghaddam, R. Maaskant, J. Yang, and P.-S. Kildal, “Characterization Method of an Automotive Random-LOS OTA Measurement Setup”, Submitted to *IEEE Transactions on Antennas and Propagation*.

**Paper 8**

**A. Razavi**, A. Alayón Glazunov, R. Maaskant, and J. Yang, “Back-of-the-envelope Evaluation of the Prevalence of RIMP or LOS Propagation as a Function of Frequency”, To be submitted.

**Other publications by the author during PhD studies**

While working as a graduate student at Chalmers, the author of this thesis has also been the author or co-author of the following publications that are not appended to the thesis.

- I **A. Razavi**, and J. Yang, “Investigation of Penetration Ability of UWB Antennas in Near-field Sensing Applications”, in *Proceedings of the 6<sup>th</sup> European Conference on Antennas and Propagation (EuCAP 2012)*, Prague, Czech Republic, March 2012.
- II **A. Razavi**, J. Yang, and T. McKelvey, “Optimal Aperture Distribution of Near-Field Antennas for Maximum Signal Penetration”, in *Proceedings of the 7<sup>th</sup> European Conference on Antennas and Propagation (EuCAP 2013)*, Gothenburg, Sweden, April 2013.
- III **A. Razavi**, R. Maaskant, J. Yang, and M. Viberg, “Optimal Aperture Distribution for Near-field Detection of Foreign Objects in Lossy Media”, in *Proceedings of IEEE-APS Topical Conference on Antennas and Propagation in Wireless Communications (APWC 2014)*, Palm Beach, Aruba, August 2014.
- IV **A. Razavi**, A. Alayón Glazunov, P.-S. Kildal, and J. Yang, “Investigation of Polarization Deficiencies in SIMO Systems in Random-LOS Propagation Channels”, in *Proceedings of the International Symposium on Antennas and Propagation (ISAP 2015)*, Hobart, Tasmania, Australia, November 2015.
- V **A. Razavi**, A. Alayón Glazunov, P.-S. Kildal, and R. Maaskant, “Array-fed Cylindrical Reflector Antenna for Automotive OTA Tests

in Random Line-Of-Sight”, in *Proceedings of the 10<sup>th</sup> European Conference on Antennas and Propagation (EuCAP 2016), Davos, Switzerland, April 2016*.

- VI A. Alayón Glazunov, **A. Razavi**, and P.-S. Kildal, “Simulations of a Planar Array Arrangement for Automotive Random-LOS OTA Testing”, in *Proceedings of the 10<sup>th</sup> European Conference on Antennas and Propagation (EuCAP 2016), Davos, Switzerland, April 2016*.



# Contents

<b>Abstract</b>	<b>i</b>
<b>Acknowledgment</b>	<b>iii</b>
<b>List of Abbreviations</b>	<b>v</b>
<b>List of Publications</b>	<b>vii</b>
<b>Contents</b>	<b>xi</b>

## I Introductory Chapters

<b>1 Introduction</b>	<b>1</b>
1.1 Antenna Characterization and Measurements . . . . .	2
1.2 Near-field Antenna Apertures . . . . .	4
1.3 OTA Measurements . . . . .	4
1.4 Thesis Outline . . . . .	6
<b>2 Near-field Focus and 3dB Near-field Beam Radius</b>	<b>9</b>
2.1 3dB Near-field Beam Radius . . . . .	10
2.2 Focal Distance and Optimal Size of Uniform Field Apertures	12
<b>3 Optimal Aperture Fields For Maximum Power Transfer in Lossy Media</b>	<b>15</b>
3.1 Problem Setup and Power Transfer Ratio . . . . .	16
<b>4 OTA Performance of Antennas in Edge Environments</b>	<b>19</b>
4.1 Rich Isotropic Multipath . . . . .	20
4.2 Random Line-Of-Sight . . . . .	21
4.3 Real-life Environment Hypothesis . . . . .	23

CONTENTS

<b>5</b>	<b>Threshold Receiver Model and MIMO Efficiency</b>	<b>25</b>
5.1	Description of The Model . . . . .	25
5.2	MIMO Efficiency . . . . .	27
<b>6</b>	<b>Multi-Antenna Systems</b>	<b>29</b>
6.1	Diversity . . . . .	29
6.2	MIMO . . . . .	30
6.3	Polarization-diversity and Polarization-MIMO Antennas . . . . .	32
<b>7</b>	<b>Summary of the Included Papers and Future Research Di- rections</b>	<b>37</b>
7.1	Future Research Directions . . . . .	40
	<b>References</b>	<b>41</b>

## II Included Papers

<b>Paper 1</b>	<b>Optimal Size of Uniform Aperture for Near-field Pen- etration Through Lossy Medium</b>	<b>53</b>
1	Introduction . . . . .	53
2	Problem Formulation . . . . .	54
3	3dB Near-field Beam Radius . . . . .	55
4	Optimal Aperture Size . . . . .	56
5	Verification . . . . .	60
6	Conclusions . . . . .	62
	References . . . . .	62
<b>Paper 2</b>	<b>Maximum Aperture Power Transmission in Lossy Homogeneous Matters</b>	<b>67</b>
1	Introduction . . . . .	67
2	Problem Description . . . . .	68
3	Optimization Procedure Formulation . . . . .	68
4	Numerical Results . . . . .	71
4.1	Basis Function Choice and Optimization Results . . .	71
4.2	Changes in Transmitter Aperture Size . . . . .	71
4.3	Transmitter and Receiver Aperture Distance Variations	74
4.4	Changes in Receiver Aperture Size . . . . .	74
4.5	Design Curves . . . . .	75
5	Conclusions . . . . .	76
	References . . . . .	77

**Paper 3 Optimal Aperture Distribution for Maximum Power**

<b>Transfer in Planar Lossy Multilayered Matters</b>	<b>81</b>
1 Introduction . . . . .	81
2 Optimization Method . . . . .	83
3 Green's Function of a Planar Multilayer Structure . . . . .	84
4 Optimization Results . . . . .	85
5 Optimal Aperture in Detection Applications . . . . .	87
5.1 MoM Formulation . . . . .	87
5.2 Effect of The Source Current Distribution . . . . .	89
5.3 Effect of The PEC Patch Size . . . . .	91
6 Conclusions . . . . .	92
References . . . . .	93

**Paper 4 Characterizing Polarization-MIMO Antennas in Random-LOS Propagation Channels**

<b>1 Introduction . . . . .</b>	<b>97</b>
2 Antenna Polarization Deficiencies . . . . .	100
2.1 Example: Two orthogonal dipoles . . . . .	101
3 Digital Threshold Receiver Model . . . . .	102
4 MIMO Efficiency . . . . .	104
4.1 One-Bitstream Case . . . . .	104
4.2 Two-Bitstream Case . . . . .	105
5 One Bitstream in $2 \times 1$ Diversity (SIMO) System . . . . .	106
6 Two Bitstreams in $2 \times 2$ MIMO System . . . . .	108
6.1 Example: Two orthogonal dipoles . . . . .	111
7 Conclusion . . . . .	113
References . . . . .	113

**Paper 5 Probability of Detection Functions of Polarization-MIMO Systems in Random-LOS**

<b>1 Introduction . . . . .</b>	<b>119</b>
2 MIMO Receiver Model and Receiver Algorithms . . . . .	121
2.1 MIMO Receiver Algorithms . . . . .	121
2.2 Ideal Digital Threshold Receiver . . . . .	122
3 Channel model . . . . .	124
4 Antenna Far-Field Orthogonalization . . . . .	126
5 Derivation of PoD functions . . . . .	127
5.1 1-bitstream SISO system . . . . .	128
5.2 1-bitstream MRC SIMO system . . . . .	129
5.3 2-bitstream ZF MIMO system . . . . .	130
6 Numerical examples . . . . .	131
7 Conclusions . . . . .	134

CONTENTS

A	Appendix - Sketch Proof of Orthogonalization of Arbitrary Far-Field vectors . . . . .	136
B	Appendix - Sketch of derivation of ZF MIMO SNR . . . . .	137
C	Appendix - Derivations of PoD functions . . . . .	138
	References . . . . .	140
	<b>Paper 6 Design of a Planar Eleven Antenna for Optimal Probability of Detection as a Wideband MIMO Micro-base Station Antenna</b>	<b>145</b>
1	Introduction . . . . .	145
2	Theory and Figure of Merit . . . . .	148
2.1	Digital Threshold Receiver Model . . . . .	148
2.2	MIMO efficiency . . . . .	149
2.3	Reference Antenna . . . . .	150
3	Modeling and Optimization . . . . .	151
3.1	Layout . . . . .	151
3.2	Optimization . . . . .	152
4	Simulation and Measurement Results . . . . .	153
4.1	Dual-Polarized 2-port MIMO Antenna . . . . .	154
4.2	Dual-Polarized 4-port and 8-port MIMO Antenna . . . . .	158
5	Conclusion . . . . .	159
	References . . . . .	160
	<b>Paper 7 Characterization Method of an Automotive Random-LOS OTA Measurement Setup</b>	<b>167</b>
1	Introduction . . . . .	167
2	Random-LOS OTA Measurement Setup . . . . .	169
3	Test zone characterization . . . . .	170
3.1	Ideal threshold receiver model and PoD . . . . .	170
3.2	Figures of merit . . . . .	171
4	Numerical Results . . . . .	171
4.1	Height effects . . . . .	174
4.2	Tilting effects . . . . .	176
4.3	Ground plane effects . . . . .	178
5	Conclusion . . . . .	180
	References . . . . .	181
	<b>Paper 8 Back-of-the-envelope evaluation of the prevalence of RIMP or LOS propagation as a function of frequency</b>	<b>185</b>
1	Introduction . . . . .	185
2	Signal Fading Model . . . . .	187
3	Scattering Model and General Assumptions . . . . .	189

4	Computation of $K$ -factor and $P_T$ . . . . .	190
5	Results . . . . .	194
	5.1 Specific assumptions . . . . .	194
	5.2 Comparison with numerical MOM-based simulations	195
6	Conclusions . . . . .	198
A	Appendix . . . . .	199
B	Appendix . . . . .	200
	References . . . . .	202



# Part I

## Introductory Chapters



# Chapter 1

## Introduction

Although electric and magnetic phenomena have been known since at least the 6<sup>th</sup> century BC, the connection between the two was unknown until 1820 when Hans Christian Ørsted noticed that the needle of a compass can be deflected from the north pole when the electric current in a nearby wire is switched on or off. The connection was further understood by the works of André-Marie Ampère, Francesco Zantedeschi and Michael Faraday, between 1820 and 1831. An important step was taken in 1860s when James Clerk Maxwell formulated the dynamic relation between electric and magnetic fields and demonstrated that associated electric and magnetic fields can travel through space as a wave. However, the existence of electromagnetic waves was not demonstrated until an experiment by Heinrich Hertz in 1888.

Parallel to these efforts, electrical communications were developed in the form of electrical telegraphy and telephony, through the works of Pavel Schilling, David Alter, Samuel Morse, Alexander Graham Bell and Thomas Edison, to name a few. Among the early milestones in electrical communications, we can name the telegraph code, duplex and multiplex telegraph, transatlantic cables, and telephone lines. However, all these systems were wired, that is, a cable had to be drawn between the two ends of the communication system. Although it is disputed as to who actually invented the wireless telegraph, Guglielmo Marconi was the first to build a complete commercial wireless telegraph system. Marconi's first successful transatlantic wireless transmission reportedly took place in December 1901 [1].

Since then wireless communications have evolved greatly. One of the components of the system, which has been present ever since, is the antenna. According to IEEE's standard for definitions of terms for antennas, the antenna is "*That part of a transmitting or receiving system that is designed to radiate or to receive electromagnetic waves*" [2]. In other words, the antenna is the device which enables the transition between a guiding device (such as transmission line or waveguide) and free-space [3]. This transition

can be in both directions, i.e., an antenna can perform both as a receiver and a transmitter. However, due to *reciprocity* of the EM wave propagation, it is sufficient only to analyze the antenna in one mode. Reciprocity is true except in some anisotropic or non-linear materials which are normally not used in antennas [4].

Marconi's receiver antenna was 150 m in height and was raised in the air with the help of kites. From such starting points the technology used in antennas and our understanding of the principles of the antennas' operation have changed dramatically. Over the time, numerous types and categories of antenna designs have been put to use. Today, antennas are used in a wide range of applications from wireless communications and radio astronomy to biomedical sensing and treatment as well as wireless power transfer.

## 1.1 Antenna Characterization and Measurements

The choice of antenna for a particular application is according to the requirements imposed by that application. These include, e.g., whether the application requires a directive antenna or an omni-directional one. Telemetry antennas are required to radiate into small areas of space, i.e., by focusing the transmitted energy at a long distance, whereas FM transmitter antennas are supposed to broadcast into all directions. Another example of the application requirements is the distance to the supposed "target": the two ends of a satellite tv link are almost 36000 kilometers apart, while in a microwave tomography system it is required to focus the power at a few centimeters distance which is often in the antenna near-field region<sup>1</sup>.

When it comes to characterizing an antenna one of the first characteristics to measure is the *far-field radiation pattern*. The far-field radiation pattern shows the angular distribution of the radiated field from the antenna in the so called far-field region of the antenna. For small antennas, the radiation pattern can be measured in an *anechoic chamber*. That is, a measurement chamber that is equipped with absorbers on the walls. By eliminating the reflections from the walls of the chamber, a Line-Of-Sight (LOS) environment is emulated, which enables us to measure only the direct radiated field and obtain accurate far-field pattern. For larger antennas, the far-field distance may be so large that indoor measurements become impractical. In such cases, outdoor measurement ranges are used where the ground reflection is controlled [5]. By measuring the radiation pattern, one

---

<sup>1</sup>The region around the antenna where the angular field distribution is dependent upon the distance from the antenna [5].

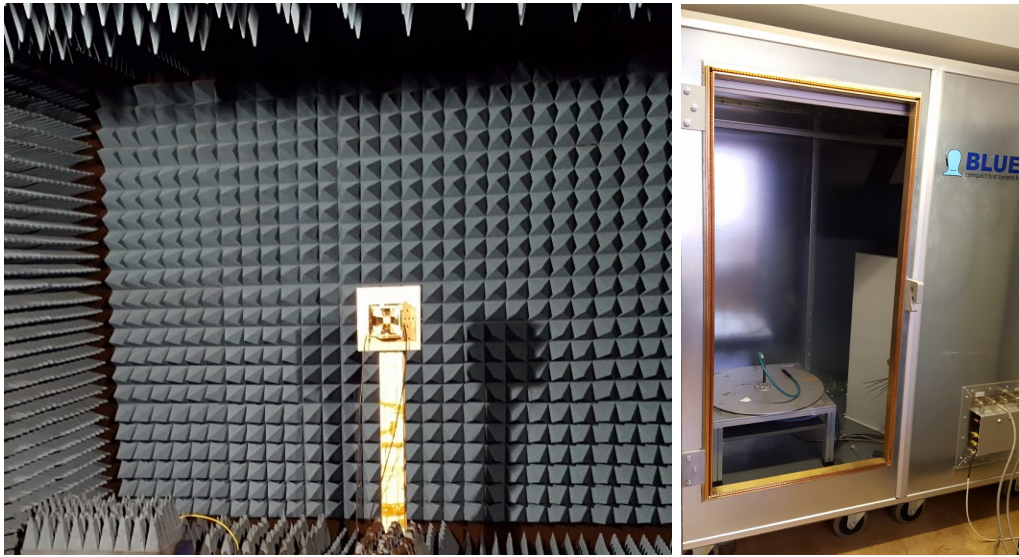


Figure 1.1: The antenna measurement chambers at Chalmers; (left) Anechoic chamber, (right) Reverberation chamber.

can obtain the *directivity* of the antenna which, as suggested by the name, is a measure of how directive the radiation pattern of an antenna is. Also, by knowing the ratio of the total radiated power to the power which is fed to the antenna, the antenna's *radiation efficiency* can be obtained.

The process of obtaining the radiation efficiency through the radiation pattern measurement is a cumbersome one. For an accurate reading, a high resolution radiation pattern measurement is required which can be very time consuming, especially when a large frequency bandwidth is concerned. A simpler way for radiation efficiency measurement is through the use of a *reverberation chamber* [6], which is a chamber fitted with reflecting walls and moving scatterers (referred to as mode stirrers) inside. By using the mode stirrers and measuring the average radiated power over time, the radiation efficiency can be measured accurately and quickly. Examples of anechoic and reverberation chambers are depicted in Fig. 1.1.

The current thesis deals with two different aspects of antenna characterization and design: The first is the characteristics and design criteria for antennas in near-field applications dealing with lossy materials, and to explore the limitations of optimal aperture antennas in these problems. The second is on the Over-The-Air (OTA) measurements of wireless devices and the Random-Line-Of-Sight (Random-LOS) environment. Random-LOS is relevant for mm-wave 5G systems, especially in small cells, and vehicular wireless communications suburban and rural environments.

## 1.2 Near-field Antenna Apertures

Traditionally, antennas have been designed and used for far-field applications. Over the years many different design concepts and antennas have been developed for wireless communications, radar, telemetry and various other applications where antenna systems interact with one another and with objects that are located in the far-field zone of the antennas. This means that the characterization of antennas in the far-field, both in fixed LOS and multipath applications, is well-defined and can be evaluated by well-developed measurement techniques [3, 4, 6].

On the other hand, in recent years, near-field microwave systems find more and more applications in recent years in areas such as detection and sensing [7–10], wireless power transfer [11], and near-field communication. In these cases, the purpose of the antenna system is to interact with the immediate surroundings, which often constitute a lossy medium. The antenna that is used in many such applications, is often designed with far-field criteria and associated limitations in mind. However, it has been demonstrated, for example in [12], that an antenna designed with good far-field properties does not necessarily provide the optimal performance in the near-field. Moreover, the characterization, design criteria, and fundamental limitations of antennas in the near-field – especially when dealing with lossy materials – have not been addressed as thorough as in the far-field. These aspects of antenna characterization and design are thus the first focus point of the present thesis. While our main aim in this part is on sensing and detection applications, some of the conclusions can be readily extended to other near-field scenarios as well.

## 1.3 OTA Measurements

Radiation pattern and efficiency measurements pertain to the antenna only. However, when it comes to the actual performance of modern communication systems with multiple antennas, the antenna alone does not determine the performance of the system. In such systems the received power from different antennas are combined with specific processing algorithms, in order to improve the system performance compared to a single antenna system. Furthermore, in some cases and particularly at millimeter wave (mm-wave) frequencies, the individual antenna ports may not even be readily accessible for measurements. Hence, it is desired to measure the performance of such systems in active mode, when the post-processing algorithms are put to action and the propagation environment is affecting the wireless link. The environment can affect the performance through the random move-

ments of objects between the transmitter and receiver, multiple reflections and multipath effects, and even the random orientation of the user device itself [13].

One option is to test the system performance in real environments. In this way, the performance of a wireless device (e.g., a cellphone) is measured while operating in various situations in the network. However, due to changes in the environment, the results of these tests can be uncontrollable and unrepeatable. OTA testing of the wireless systems is therefore used with the objective to evaluate the system's performance in a reliable and realistic way [14]. During OTA measurements, a link is established in an emulated propagation environment by using a communication tester. The system's performance is then measured in practice in terms of, e.g., data throughput.

Depending on the intended application of the wireless system, the choice of propagation environment and the way it is emulated play a major role in the accuracy and reliability of OTA measurements. To this day, various setups and methods are proposed for OTA measurements. Reverberation chambers are used to emulate a Rich Isotropic MultiPath (RIMP) environment for testing small antennas [15, 16]. In addition, multiprobe test setups in anechoic chambers are also proposed [14, 17], which can emulate non-isotropic multipath environments.

For 5G systems, the use of many small cells and mm-wave links to moving users are foreseen. Furthermore, massive MIMO and beam forming are expected to be used heavily in 5G networks. The combined effect of smaller cells, multi-user beam forming, higher directivity of the antennas, and higher penetration losses, leads to LOS being more pronounced compared to the current mobile networks. Another area where LOS is more pronounced is the automotive industry. The growth in the use of music streaming services, navigation systems with live traffic information, and safety features that may require data connection, leads to the need for high capacity wireless links to vehicles. In rural and suburban areas a LOS link is often present between the vehicle and the base station. In the aforementioned scenarios, unlike fixed LOS systems such as mobile backhaul microwave links, the orientation of the user terminal is random. Hence, although only one direct path is present between the transmitter and the receiver, the Angle of Arrival (AoA) and polarization (in the case of mobile systems) of the waves are random. The term Random-LOS is introduced in order to distinguish this scenario from traditional fixed LOS [18, 19]. A distinction between the two scenarios is the AoA distribution. The AoA is random in the horizontal plane in the case of vehicles, whereas for mobile systems it is over the whole 3D sphere.

The fact that random orientation of the user terminal affects the performance of diversity systems has been known since the 80's [13,20]. However, it has not been investigated as thoroughly as the effects of multipath. Similarly, for OTA measurements, characterization of antennas in the RIMP environment are already well-studied and understood [16]. Whereas, the Random-LOS OTA measurement is relatively new and less understood. The Random-LOS environment, performance of MIMO systems in this environment, and OTA measurement setups for the Random-LOS are thus the second focus point of this thesis.

## 1.4 Thesis Outline

The thesis is divided into two main parts. Part I, which consists of 7 chapters, offers a background of the research topic and introduces concepts and tools upon which the research work is based. Chapters 2 and 3 are dedicated to a background on optimal near-field apertures in lossy media, followed by Chapters 4, 5, and 6, which cover the OTA measurements and Random-LOS environment.

We deal with the focusing of power in the near-field in Chapter 2. The axial pattern, which is traditionally used to characterize the antenna focus in near-field, is the intensity of the E-field on the axis of the antenna aperture. The axial pattern does not efficiently characterize the antenna in the presence of losses in the media. In this chapter, the 3dB near-field beam radius is introduced as a mean of characterizing the antenna's performance in focusing the radiated power in the near-field.

Chapter 3 presents a method for finding the optimal aperture field distribution for maximizing the near-field power coupling between a pair of antennas, which is beneficial for both the detection of foreign objects as well as for the optimal power transfer and near-field communication in lossy media.

In Chapter 4 a systematic approach is introduced to characterize the performance of wireless systems in two edge OTA scenarios. A real-life hypothesis is presented which relates the actual performance of the system in a real-life environment to the performance measurements in these two extremes. The actual propagation environment is expected to be somewhere in-between these two extremes.

When simulating antenna systems in RIMP or Random-LOS it is convenient to determine the received power by the antenna and the corresponding probability distribution. Whereas in OTA measurements system data throughput is a common metric to use. We use the ideal digital threshold receiver model to relate the probability distribution of the received power to

the normalized system throughput or Probability of Detection (PoD). The threshold receiver model and its application in RIMP and Random-LOS are described Chapter 5.

Chapter 6 is dedicated to multi-antenna systems. In these systems different post-processing algorithms which can be used to combine the output of individual antennas in diversity and MIMO systems. These algorithms are introduced in this chapter.

Part II of the thesis consists of 8 research papers, 3 of which are on the near-field apertures topic and 5 on the Random-LOS environment.

The different aspects of antenna characterization, in the near-field and the Random-LOS environment, that are covered in the attached papers are:

1. Characterization of the near-field focus of aperture antennas in lossy media,
2. Determining the optimal aperture field distribution for maximum power transfer in near-field,
3. Characterization and requirements in the design of polarization-MIMO antennas for optimum performance in Random-LOS,
4. Study and characterization of a test chamber antenna for Random-LOS automotive OTA measurements, and
5. Evaluation of the prevalence of RIMP or LOS propagation as a function of frequency.

Part I ends with Chapter 7 which summarizes the contributions of the included papers in more details and provides some of the possible future extensions of the work.



## Chapter 2

# Near-field Focus and 3dB Near-field Beam Radius

Since the 1950's there has been studies on the so-called "Focused apertures". In a "focused aperture", a spherical phase front is employed to focus the energy of the field at a certain distance in the Fresnel zone [21, 22]. It was shown that on the focal plane, near its axis, the electric field of a focused aperture exhibits several properties of the far-field. For example, a tapered aperture distribution results in decreased sidelobe levels, increased beamwidth, and a decreased gain. In addition, it has been shown that the actual location of the maximum field intensity along the axis of the aperture is not exactly at the intended focal distance set by the aperture phase distribution. The corresponding offset is dependent on the size of the aperture and the focal distance [21]. On the other hand, it has been pointed out that an inverse taper results in low forelobes and aftlobes<sup>1</sup>, but also to high sidelobes and a large reduction in gain [22]. The axial pattern of focused antennas can be synthesized by using methods similar to those used for synthesizing far-field patterns, where the focal distance is controlled separately by the aperture phase distribution. The control over the axial pattern comes at the cost of a degradation in the angular or transverse pattern as an increase in the width of the main beam or an increase in the sidelobe level [23]. Successful attempts in realizing focused apertures have been made by employing large microstrip arrays or Fresnel zone plate lenses [24, 25]. However, none of the above-mentioned earlier works have taken losses in the medium into account in their investigations.

Axial pattern, i.e., the intensity of the electric field on the axis of the aperture, is often used in the aforementioned works. Fig. 2.1 shows the E-field intensity on the axis of a circular uniform aperture of radius  $4\lambda$  in three

---

<sup>1</sup>Forelobes and aftlobes are defined as the axial lobes before and after the focal distance, respectively [22].

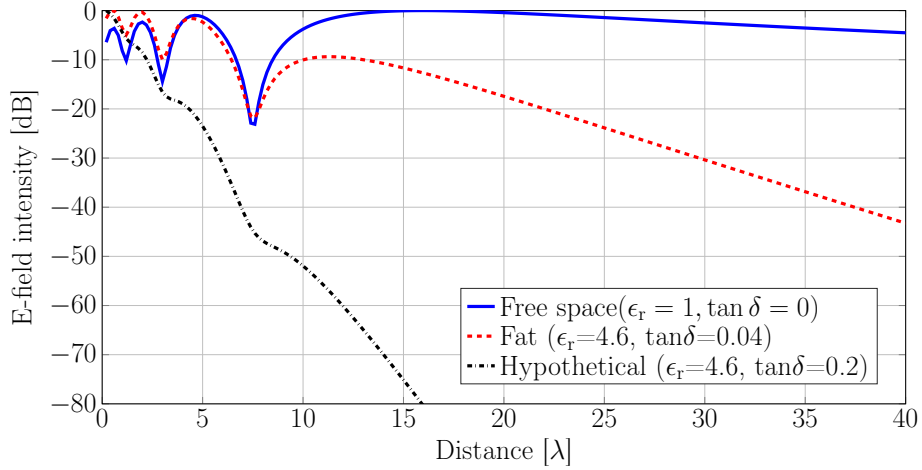


Figure 2.1: The E-field intensity on the axis for a circular uniform field aperture of radius  $4\lambda$  vs. distance from the aperture in three different media.

media, each with a different conductivity. As can be seen in this figure, as soon as loss is introduced to the medium, the axial pattern, forelobes and aftlobes cannot be defined any longer. This means that new characteristics need to be defined and used.

## 2.1 3dB Near-field Beam Radius

The field radiated by a circular uniform field aperture of radius  $5\lambda$ , located in the  $xy$ -plane at  $z = 0$  in brain tissue ( $\epsilon_r = 57.5, \sigma = 1.22$  S/m at 1 GHz [26]), is plotted in Fig. 2.2 for two different normalization schemes. In the first plot, the E-field intensity is normalized to the overall maximum and demonstrates a rapid attenuation with distance from the aperture due to losses in the medium. Whereas, the E-field intensity in the latter is normalized separately at each plane parallel to the aperture. The source is assumed to be a  $y$ -polarized Huygens source. As can be observed in this simple illustration, although the field intensity is attenuated heavily with an increase in distance from the aperture, the focus of the available power varies along the axis of the aperture. For example, the uniform aperture in this case has its narrowest focus around a distance of  $23\lambda$  from the aperture. This leads us to the definition and use of the 3dB near-field beam radius.

The 3dB near-field beam radius is defined as the radius of the smallest circle on each plane parallel to the aperture, which contains all field points where the field strength (intensity of E-field) is higher than -3dB of the highest intensity value in that plane. In other words, all field points outside

## 2.1. 3dB NEAR-FIELD BEAM RADIUS

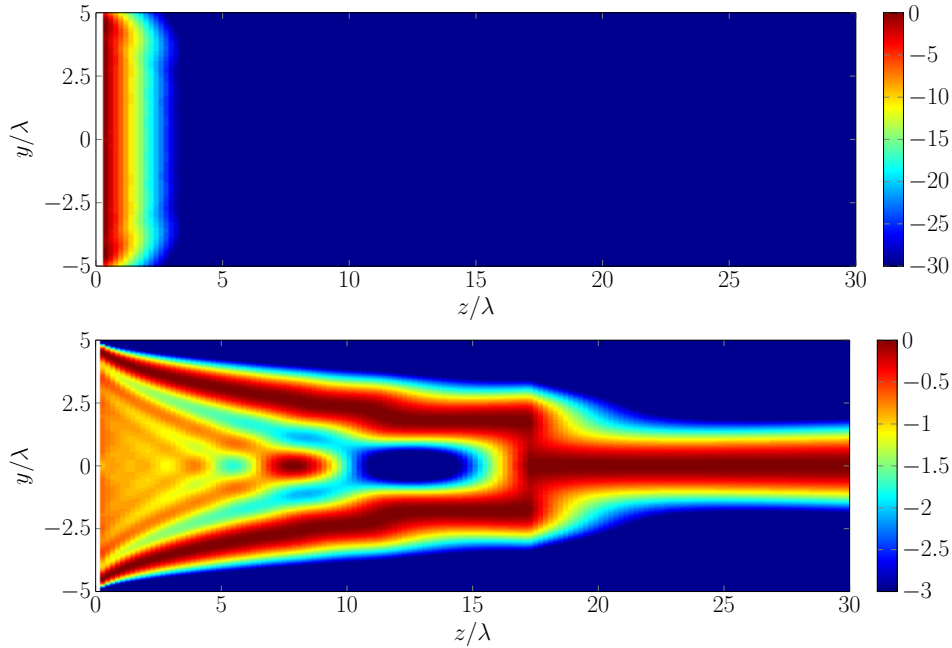


Figure 2.2: The E-plane field intensity (in dB) of a circular uniform aperture in brain tissue, normalized to the overall maximum (top), and normalized at each plane parallel to the aperture (bottom). The aperture is located at  $z = 0$ .

this 3dB-beam circle have a field strength below -3dB of the strongest value in that plane. The center of the 3dB-beam circle is always on the symmetry axis of the aperture. Note that, although the word “beam” is used in the definition, a beam in the classical antenna sense may not really be formed in the near-field of an antenna. The 3dB near-field beam radius, which is denoted by  $r_{3\text{dB}}$ , is measured in terms of millimeters or wavelengths, which is different from the 3dB beamwidth used to characterize the far-field radiated beam which is usually measured in degrees. Fig. 2.3 illustrates the definition of the 3dB near-field beam radius for two  $z$ -plane cuts carrying different field distributions.

It is noteworthy that the 3dB beam radius is independent of the type of the current sources, i.e., electric, magnetic, or Huygens source. To understand this independence, we should bear in mind that the 3dB beam radius is defined based on the relative field intensity (compared to its maximum). The equality of the beam radius for electric and magnetic currents can be explained through the duality theorem [27, pp:310-312]. The equality of the beam radius for the Huygens source with the others is explained by the fact that the electromagnetic fields are linear functions of the current sources and superposition can be applied to them.

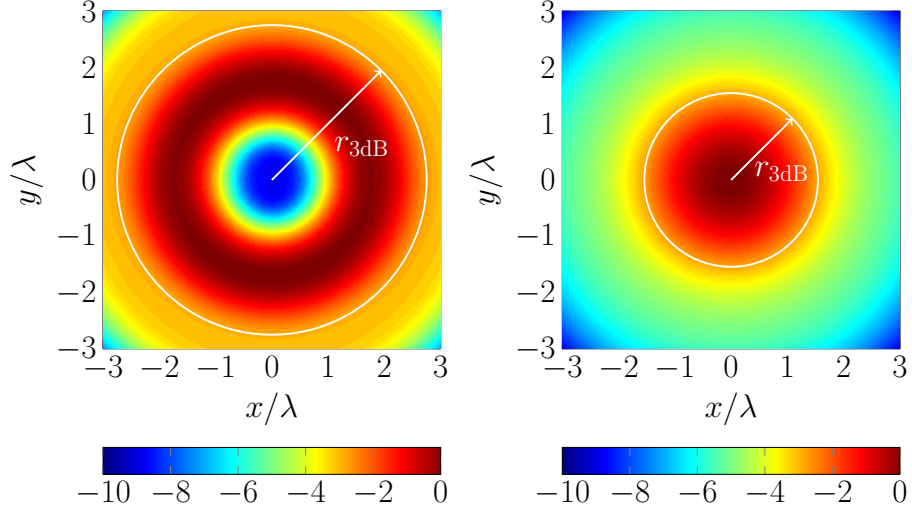


Figure 2.3: Illustrating the definition of the 3dB near-field beam radius through the white circle for two different field distributions, where the maximum on the plane is located off-center (left) and at its center (right) of the 3dB circle.

## 2.2 Focal Distance and Optimal Size of Uniform Field Apertures

The 3dB beam radius can be used to determine the optimal size of uniform apertures for near-field sensing applications in lossy media. For this purpose, we assume circular apertures of radius  $a$  in  $xy$ -plane in homogeneous medium, as shown in Fig. 2.4. The aperture supports a uniform  $y$ -polarized electric current ( $\mathbf{J}$ ) distribution,

$$\mathbf{J}(\mathbf{r}') = C\hat{\mathbf{y}}, \quad |\mathbf{r}'| \leq a, \quad (2.1)$$

where  $C$  is an arbitrary scalar constant. The radiated field is then obtained by using the integral expressions in [4, Sec. 4.2.1], i.e.,

$$\mathbf{E}_J(\mathbf{r}) = C_k \eta \iint_{S'} \left[ \mathbf{J} C_{N1} - (\mathbf{J} \cdot \hat{\mathbf{R}}) \hat{\mathbf{R}} C_{N2} \right] \frac{1}{R} e^{-jkR} dS' \quad (2.2)$$

with  $\eta = \sqrt{\mu/\epsilon}$  as the wave impedance,  $k = 2\pi/\lambda$  as the wavenumber and

$$\begin{aligned} \mathbf{R} &= \mathbf{r} - \mathbf{r}', \quad R = |\mathbf{r} - \mathbf{r}'|, \quad \hat{\mathbf{R}} = \frac{\mathbf{R}}{R}, \quad C_k = \frac{-jk}{4\pi}, \quad C_N = 1 + \frac{1}{jkR}, \\ C_{N1} &= 1 + \frac{1}{jkR} - \frac{1}{(kR)^2}, \quad C_{N2} = 1 + \frac{3}{jkR} - \frac{3}{(kR)^2}. \end{aligned}$$

## 2.2. FOCAL DISTANCE AND OPTIMAL SIZE OF UNIFORM FIELD APERTURES

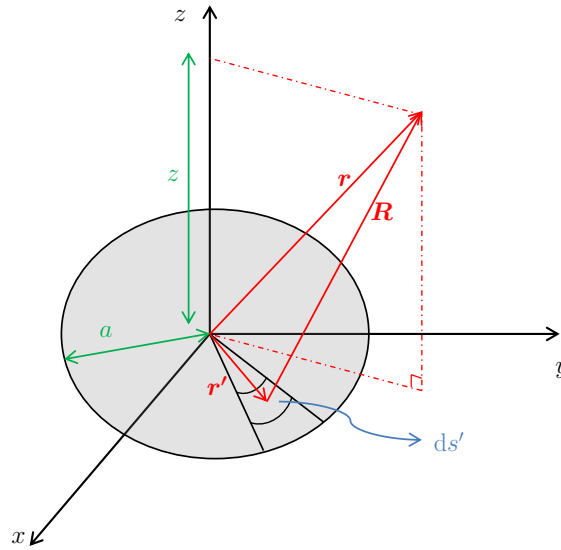


Figure 2.4: A circular aperture in  $xy$ -plane.

The 3dB beam radius can then be calculated for different uniform aperture sizes and in different media. As an example, the 3dB near-field beam radius of uniform field circular apertures of different radii are plotted in Fig. 2.5. It is observed in this figure that for any aperture size, there is a certain distance ( $z_{\min}$ ) where the beam radius ( $r_{3\text{dBUA}}$ ) attains its smallest value. Beyond this distance, the beam transforms into a far-field beam and the beam radius increases at a constant rate.

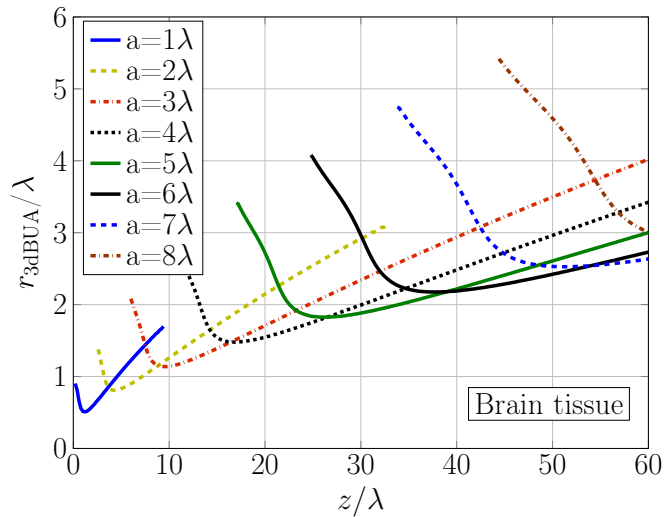


Figure 2.5: 3dB near-field beam radius of uniform field circular apertures of different radii in brain tissue.

In a through-sensing system, i.e., when two antennas are positioned on the opposite sides of the lossy material, the scattering from a foreign object will be the strongest if the object is located at a depth around  $z_{\min}$ . This is because  $z_{\min}$  is the depth where the focus size is the smallest. Hence, by knowing the location and the size of the focus for each aperture size in a given media, one can find its optimal size for each application based on the depth of interest. To this end, we have investigated the effect of the medium properties and the size of the aperture on  $z_{\min}$ , and the beam radius at the focal point  $r_{3\text{dBmin}}$  in Paper 1. Empirical formulas are presented for  $z_{\min}$  and  $r_{3\text{dBmin}}$  as functions of the aperture radius and the loss tangent of the medium. The optimal size of the uniform aperture for the detection of foreign objects in lossy media, as well as the effect of a correctly chosen aperture size on the scattered power from objects are investigated and presented in this paper with an idealized test setup.

## Chapter 3

# Optimal Aperture Fields For Maximum Power Transfer in Lossy Media

In the previous chapter we introduced and discussed the 3dB near-field beam radius and its relation to the antenna focus in the near-field for the case of homogeneous lossy media. It was subsequently used to find an optimal size of a uniform aperture for the detection of foreign objects. In the present chapter we will take another approach to the synthesis of the optimal aperture field problem, that is, to numerically find the optimal aperture distribution that maximizes the power coupling between two antennas separated by a lossy medium, given a fixed receiver size and antenna separation distance. The applications for such optimal apertures include, but are not limited to, wireless power transfer to implants and in-body communication with these implants, where the receiver is typically very small. It is argued that maximizing the power coupling between two antennas will enhance the detection probability of foreign objects in sensing applications, since the disturbance in the presence of any foreign object is likely to be maximized as well [28, 29].

Kay [30] has investigated the near-field gain of aperture antennas in an attempt to maximize it. However, the analytical approach in [30] leads to integral equations which should be solved numerically and due to limited computational resources was deemed inconvenient in the time. Borgiotti [31] has used the reaction integrals in order to formulate and maximize the power transfer between two planar apertures in the near-field. However, the field distribution in the latter work can be analytically solved only in the particular case of rectangular apertures. The present numerical approach has the advantage of being applicable to different aperture geometries.

### 3.1 Problem Setup and Power Transfer Ratio

The problem setup is illustrated in Fig. 3.1. Two antennas are separated by a lossy medium with a complex-valued characteristic impedance  $\eta$ . The objective is to find an electric ( $\mathbf{J}$ ) and magnetic ( $\mathbf{M}$ ) current distribution that maximizes the ratio of the received power to the total input power. Since the medium is lossy, the effect of the backscattered field from the receiving side on the transmitting side can be neglected. Hence, one can assume that the source currents  $\mathbf{J}$  and  $\mathbf{M}$  radiate in a homogenous medium with characteristic impedance  $\eta$ . The total received power  $P_{\text{out}}$  is given by

$$P_{\text{out}} = \frac{1}{2} \Re \left\{ \int_{S_2} [\mathbf{E}(\mathbf{J}, \mathbf{M}) \times \mathbf{H}^*(\mathbf{J}, \mathbf{M})] \cdot \hat{\mathbf{n}}_2 \, dS \right\}. \quad (3.1)$$

Similarly, the supplied power  $P_{\text{in}}$  is given by

$$P_{\text{in}} = \frac{1}{2} \Re \left\{ \int_{S_1} [\mathbf{E}(\mathbf{J}, \mathbf{M}) \times \mathbf{H}^*(\mathbf{J}, \mathbf{M})] \cdot \hat{\mathbf{n}}_1 \, dS \right\}. \quad (3.2)$$

Next if we expand  $\mathbf{J}$  and  $\mathbf{M}$  in terms of  $N$  basis functions as

$$\mathbf{J} = \sum_{n=1}^N j_n \mathbf{f}_n(\mathbf{r}), \quad \mathbf{M} = \sum_{m=1}^N m_m \mathbf{g}_m(\mathbf{r}) \quad (3.3)$$

and substitute (3.3) in (3.1) and (3.2), the supplied and received powers can

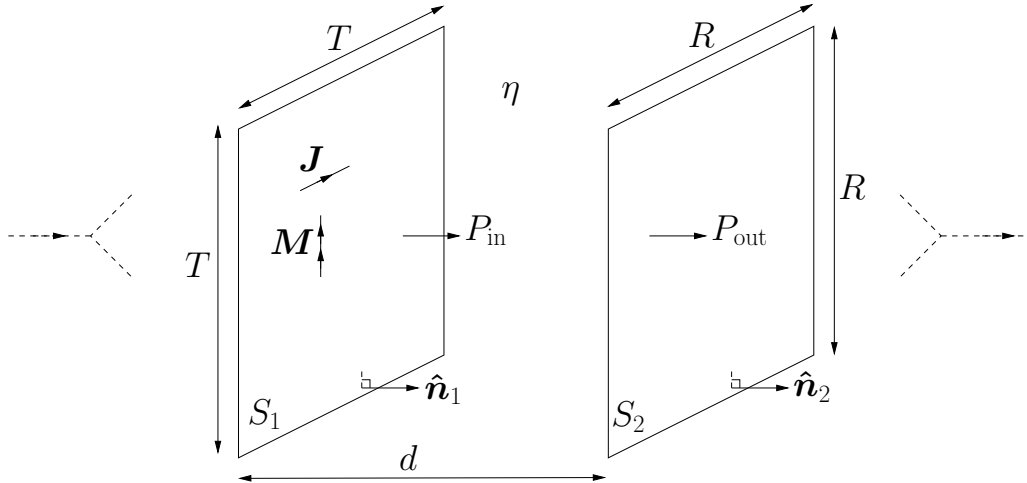


Figure 3.1: Problem setup including a transmitting and an ideally receiving aperture antenna.

### 3.1. PROBLEM SETUP AND POWER TRANSFER RATIO

be written after some manipulations as

$$P_{\text{out}} = \frac{1}{2} \Re\{\mathbf{w}^H \mathbf{P}_{\text{out}} \mathbf{w}\} \quad (3.4a)$$

$$P_{\text{in}} = \frac{1}{2} \Re\{\mathbf{w}^H \mathbf{P}_{\text{in}} \mathbf{w}\} \quad (3.4b)$$

where  $\mathbf{P}_{\text{in}}$  and  $\mathbf{P}_{\text{out}}$  are system matrices for the input and output powers, and where  $\mathbf{w}$  is the vector containing the unknown weights  $j_n$  and  $m_m$  of the basis functions, i.e.,

$$\mathbf{w} = \begin{bmatrix} \mathbf{j} \\ \mathbf{m} \end{bmatrix}.$$

The derivation of  $\mathbf{P}_{\text{in}}$  and  $\mathbf{P}_{\text{out}}$  in (3.4) is explained in detail in Paper 2 and is therefore omitted in this chapter to avoid repetition. The objective is to maximize the ratio of the received power to the supplied input power, or power transfer ratio ( $P_{\text{tr}}$ ), which can be written as

$$P_{\text{tr}} = \frac{P_{\text{out}}}{P_{\text{in}}} = \frac{\Re\{\mathbf{w}^H \mathbf{P}_{\text{out}} \mathbf{w}\}}{\Re\{\mathbf{w}^H \mathbf{P}_{\text{in}} \mathbf{w}\}} = \frac{\mathbf{w}^H [\mathbf{P}_{\text{out}} + \mathbf{P}_{\text{out}}^H] \mathbf{w}}{\mathbf{w}^H [\mathbf{P}_{\text{in}} + \mathbf{P}_{\text{in}}^H] \mathbf{w}}. \quad (3.5)$$

The objective is to find  $\mathbf{w}$  which maximizes (3.5) at a stationary point, which leads to the generalized eigenvalue equation

$$[\mathbf{P}_{\text{out}} + \mathbf{P}_{\text{out}}^H] \mathbf{w} = P_{\text{tr}} [\mathbf{P}_{\text{in}} + \mathbf{P}_{\text{in}}^H] \mathbf{w}. \quad (3.6)$$

Hence, maximizing (3.5) is equivalent to finding the largest eigenvalue  $P_{\text{tr}}$  in (3.6), provided that  $\mathbf{P}_{\text{in}} + \mathbf{P}_{\text{in}}^H$  is a positive definite matrix. This condition can be achieved by, e.g., employing Huygens source basis functions which constrain the input power to positive values.

As an example, we apply the above described method to a pair of  $2\lambda \times 2\lambda$  apertures, which are separated by a distance of  $4\lambda$ , assuming the surrounding medium is muscle tissue ( $\epsilon_r = 57$ ,  $\sigma = 1.2$  S/m at 1 GHz [32]). The receiving antenna is assumed to be conjugate impedance and field matched to the receiving aperture fields, thereby harvesting all the power passing through it. We employ a rectangular grid of pulse basis function currents and assume an  $x$ -polarized electric aperture field. The basis function currents modeled as

$$\mathbf{f}_n(\mathbf{r}) = \hat{\mathbf{x}}\Pi(\mathbf{r}_n) \quad \text{and} \quad \mathbf{g}_n(\mathbf{r}) = \hat{\mathbf{y}}\Pi(\mathbf{r}_n) \quad (3.7)$$

where  $\Pi(\mathbf{r}_n)$  is the support of the  $n$ th pulse basis function of size  $(0.1\lambda)^2$  with centroid  $\mathbf{r}_n$ . Furthermore, we restrict the currents to Huygens source, i.e.,  $m_n = \eta j_n$ . The normalized amplitude and phase of the optimized electric

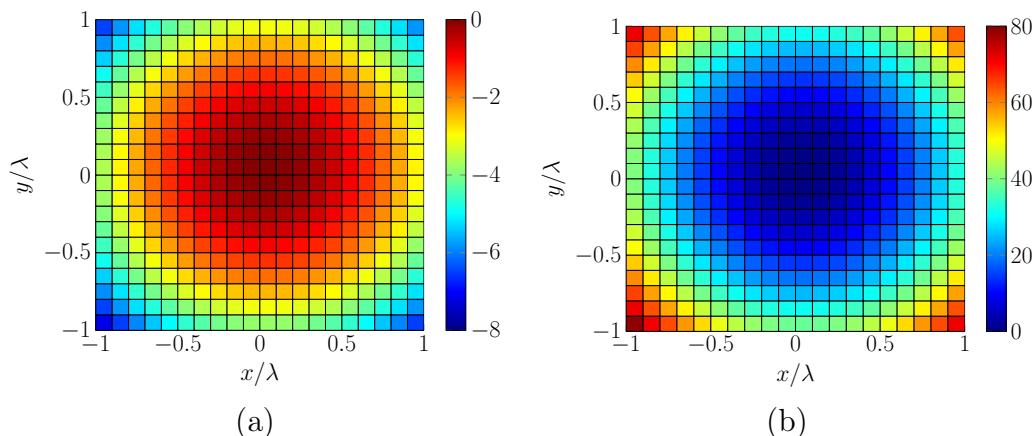


Figure 3.2: (a) Amplitude in dB and, (b) phase in degrees, of the optimized electric current distribution on the transmitter aperture. The transmitter and receiver aperture sizes are  $2\lambda \times 2\lambda$ , located  $4\lambda$  away from one another.

currents are plotted in Fig. 3.2. The distribution of the phase has a phase lead towards the edges of the aperture which contributes to achieving a focused beam in the near-field at the receiver antenna's position. The amplitude distribution has a concentration of power around the center of the transmitter aperture which contributes to a reduction in path attenuation and an increase in the power transfer ratio.

The details on determining  $\mathbf{P}_{\text{in}}$  and  $\mathbf{P}_{\text{out}}$  matrices are described in Paper 2. The methodology that is presented here is used in this paper to determine general properties of optimal apertures and limitations on optimal power transmission in homogeneous lossy media. Although the formulation was originally derived for homogeneous media, it can be easily extended to any non-homogeneous media as long as the Green's function of the emanated fields from the basis functions are known for the structure. We have used G1DMULT [33] algorithm to obtain the emanated fields from the basis functions in multi-layered lossy media, and to obtain the optimal aperture distribution in Paper 3. Furthermore, it is shown in this paper that maximizing the power transfer ratio will lead to higher sensitivity for detection of foreign unwanted objects in the lossy environment.

## Chapter 4

# OTA Performance of Antennas in Edge Environments

In OTA measurements, a communication tester is used to establish a link to the device under test in an emulated propagation environment. In this case the emulated propagation environment plays a key role in the reliability of the test. Ideally, for a given application, frequency and propagation environment, an accurate model of the propagation needs to be obtained and emulated in a controlled and repeatable way. Various setups and methods are proposed for emulation of the propagation environments. For example, reverberation chambers are used to emulate a RIMP environment for OTA measurements [15, 16], or multiprobe test setups in anechoic chamber are proposed [14, 17] to emulate non-isotropic multipath environments.

It is a common practice to study the performance of a system at its operating extremes, in order to gain insight into the behavior of the system within the expected working range. For example, in electric circuit theory, an RC circuit can be characterized by analyzing it at DC and at a high frequency, which gives an impression of the filtering characteristic of the circuit. By taking a similar approach, instead of modeling and emulating typical propagation environments, we define two extreme propagation environments and perform the OTA testing in these two. The two extreme environments, referred to as edge environments, are chosen with respect to the number of multipath components and their spatial distribution. These two are the Rich Isotropic MultiPath (RIMP) and Random Line-of-Sight (LOS) environments. An overview of these two is provided below.

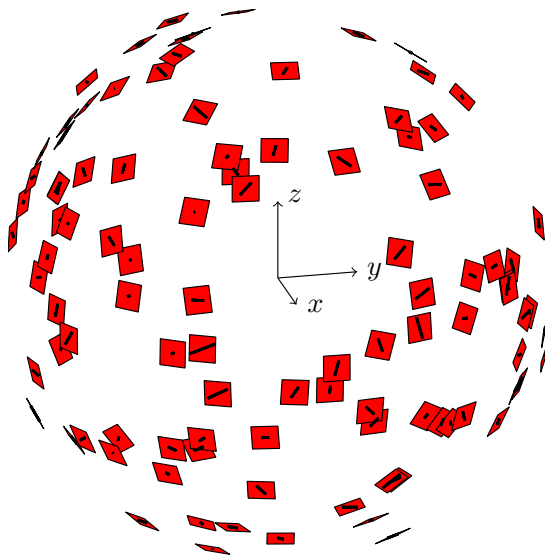


Figure 4.1: Illustration of RIMP random plane waves. The AUT is located at the center of the coordinate system. Each red patch represents a plane wave with random AoA, polarization, amplitude and phase.

## 4.1 Rich Isotropic Multipath

The first edge environment is the Rich Isotropic MultiPath (RIMP) environment. Here, the term rich refers to the number of multipath components, where many (typically more than 20 [4]) simultaneous incoming plane waves are assumed impinging on the antenna under test (AUT). Furthermore, isotropic refers to the angular distribution of these plane waves, which are assumed to be uniformly distributed over the solid angle of  $4\pi$  sr, as illustrated in Fig. 4.1. Under these conditions, the magnitude of the voltage received by a lossless antenna in RIMP has a Rayleigh probability distribution.

In the multipath environment the radiation pattern and directivity of single-port antennas do not play a large role in the statistics of the received signal, as opposed to LOS. That is because many interfering waves with arbitrary AoA, polarization, amplitude and phase contribute to the resulting signal at the antenna port. The cumulative distribution function (CDF) of the received power by two different antennas in RIMP are compared to the Rayleigh distribution in Fig. 4.2. It is evident that, as long as both antennas have equal efficiency, their corresponding radiation patterns are irrelevant to the distribution of the received power. On the other hand, the radiation pattern of multi-port antennas plays a fundamental role in the distribution of the received power since it contributes to the correlation between the ports.

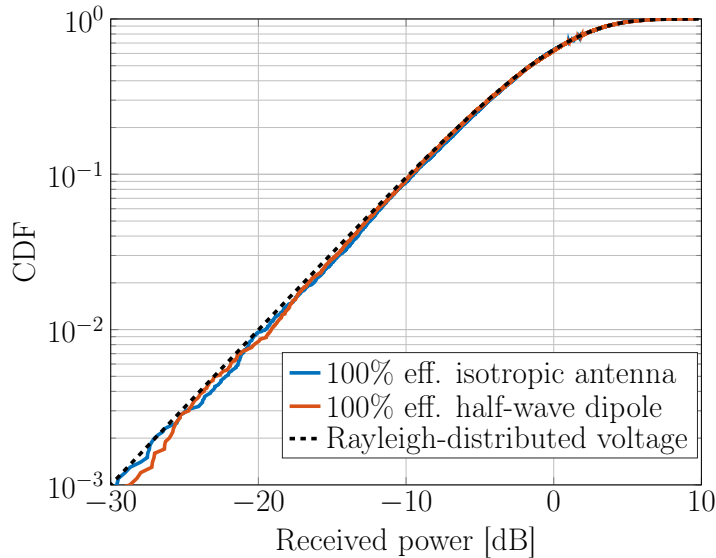


Figure 4.2: The CDF of the received power by two lossless antennas in RIMP.

RIMP environment is readily emulated in a reverberation chamber. Reverberation chambers were traditionally used for testing electromagnetic compatibility (EMC), but they have since found new applications in characterization of small antennas and active OTA measurements in multipath. For example, total radiation efficiency measurements can be performed in reverberation chambers with good accuracy and in shorter time compared to full radiation pattern measurements in anechoic chambers [34].

Perhaps more importantly, reverberation chambers have found application in active OTA measurements of system performance in terms of diversity gain, capacity and throughput for diversity and MIMO systems [16]. In this role, the reverberation chamber is used to emulate a multipath channel and with a communication tester a wireless link is established, which makes active performance measurements of a wireless system possible. The parameters of the emulated channel in a reverberation chamber can be controlled by modifications in chamber's design. For example, while the channel in an unloaded reverberation chamber is Rayleigh distributed [35], by loading the chamber Rician fading can also be achieved [36–38]. The delay spread and Doppler spread in reverberation chambers are also studied in [39–42].

## 4.2 Random Line-Of-Sight

As mentioned earlier, we consider LOS as the second edge environment. Traditionally the LOS channel has been relevant in fixed links such as mobile

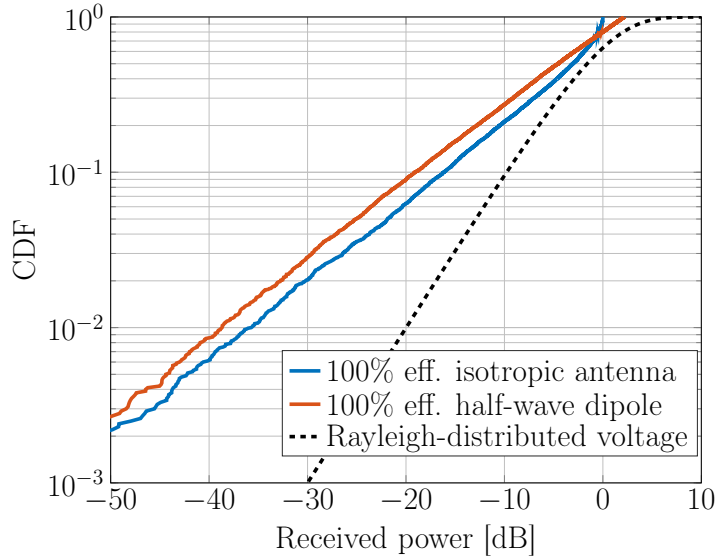


Figure 4.3: The CDF of the received power by two lossless antennas in Random-LOS.

backhaul wireless links, and has been considered a fixed and deterministic channel. The 5G wireless systems are expected to include communications to the users via mm-wave links. At mm-wave frequencies, the multipath is less pronounced and the LOS channel gradually takes the dominant role. LOS is also expected to play a dominant role in wireless links to and from vehicles, especially in rural areas and on highways, where there often is a LOS path between the antenna on the car and the base-station antenna. However, unlike the antennas in fixed installations, the orientation of the vehicle on the road or a mobile terminal is random [19]. Therefore, although there may be only one propagation path between the transmitter and the receiver, its polarization and Angle of Arrival (AoA) are random. To distinguish this scenario from traditional fixed LOS, we use the term Random-LOS [18, 43]. For mobile terminals, the AoA has a random 3D spatial distribution and the polarization is also random. Whereas in the automotive case, the AoA has almost a 2D spatial distribution and the polarization has much less variations.

The randomness in the Random-LOS environment causes slow fading, as compared to the fast fading in the Rayleigh environment. Random-LOS can be modeled in simulations by a single incoming wave with fixed amplitude and uniformly distributed AoA and polarization angle. Unlike the RIMP scenario, the fading is determined by the antenna radiation pattern in Random-LOS. The effect of the radiation pattern is demonstrated in

Fig. 4.3, which shows the CDF of the received power for the same antennas as in Fig. 4.2, but this time in the Random-LOS environment.

Antenna systems which are intended for the mm-wave 5G bands or automotive applications must be designed to account for the slow fading of the Random-LOS environment. For OTA measurements of these systems, Random-LOS can be emulated in anechoic chambers. Active OTA measurements of automotive antennas in Random-LOS have been performed in anechoic chambers and show good agreement with simulation results [44,45].

### 4.3 Real-life Environment Hypothesis

For real-life channels, knowing exactly what channel model is the typical one, or the most representative, is in general not fully possible. RIMP and Random-LOS represent the edges of the real-life channels. Hence, the two aforementioned edge environments can be used to characterize the antenna system. The relationship between the performance of a system in a real-life environment, to its performance in the two edge environments is formulated as a working hypothesis in [18]. The real-life hypothesis for OTA device characterization states: *“If a wireless device is proven to work well in both RIMP and Random-LOS, it will work well in real-life environments”*.

The real-life hypothesis remains to be rigorously proven. However, it is so far supported by experimental observations [46]. In another example, it is argued that both edge environments are favorable for Massive MIMO systems [47]. The real propagation environment is likely to be in-between the two edge environments and it is reasonable to expect it to be favorable as well. Favorable propagation conditions means that the channel vectors between the users and the base-station are nearly pairwise orthogonal. Therefore, it is a desirable scenario where the signal processing complexity can be considerably reduced and the throughput can be maximized.



# Chapter 5

## Threshold Receiver Model and MIMO Efficiency

Electromagnetic simulation tools provide us with the radiation pattern and the radiation efficiency of the antenna. It is desirable to use this information to gain insight into the system OTA performance. There are other instances where performing OTA measurements is not readily possible. In these cases the output power at the antenna port, or rather its CDF, may be more readily available than the throughput in the wireless system. For example, a communication tester may not be always at hand to emulate the base-station modulation and coding in an OTA measurement setup. In another example, when designing a new antenna for already-available electronics, it may be more convenient to estimate the complete system performance by measuring only the received power at the antenna port before integrating it in the system. The *ideal digital threshold receiver model* [48] is a model which relates the CDF of the output power at the antenna port to the Probability of Detection (PoD) in the communication system. This model is described below.

### 5.1 Description of The Model

In a communication system, the PoD is the probability of receiving a bitstream at the receiver with no errors. The ideal digital threshold receiver model is used to determine the PoD from the CDF of the received power. It was originally introduced to model the throughput of digital communication systems in the RIMP environment [49], but it has since found application in Random-LOS as well [45]. The ideal threshold receiver model is based on the simplified assumption that in modern digital communication systems the error rate (i.e., the failure to detect a bitstream) will abruptly

change from 100% (all errors) to 0% (no error) in a stationary Additive White Gaussian Noise (AWGN) channel. This is true in practice, due to the use of advanced error correction schemes. This means that, as soon as the received signal-to-noise ratio (SNR) or the received power reaches a certain threshold level, the error rate will drop to 0%. The threshold level is dependent on the receiver design and the wireless system specifications. It can be determined by conductive measurements, where the communication tester is connected directly to the receiver by a cable, if a measurement port is available at the device.

According to the ideal threshold receiver model, the PoD can be written as [48]:

$$\text{PoD}(P/P_{\text{th}}) = \frac{\text{TPUT}(P/P_{\text{th}})}{\text{TPUT}_{\text{max}}} = 1 - \text{CDF}(P_{\text{th}}/P), \quad (5.1)$$

where  $P_{\text{th}}$  is the threshold level of the receiver,  $P$  is a reference value proportional to the transmitted power, PoD is the Probability of Detection function, TPUT is the average throughput, and CDF is the Cumulative Distribution Function (CDF) of the received fading power  $P_{\text{rec}}$  normalized to the reference ( $P_{\text{rec}}/P$ ). In the case when the received power does not undergo fading, the PoD is a step centered on the threshold level, i.e., for  $P = P_{\text{th}}$ . The power values relative to  $P_{\text{th}}$  are shown in dBt, which is the dB value relative to the threshold level of the receiver itself.

In the RIMP case the received power undergoes Rayleigh fading. Hence, the CDF in (5.1) is described by the Rayleigh probability distribution function. The average power of the Rayleigh distribution is then used as the reference power in RIMP, i.e.,  $P = P_{\text{av}}$ . In the Random-LOS case where we deal with random polarization and AoA, the maximum received power is used as the reference value, i.e.,  $P = P_{\text{max}}$ . The maximum received power occurs when the polarization of the receiver is aligned with that of the incident wave.

We will illustrate the digital threshold receiver by an example of a lossless isotropic antenna in the RIMP environment. The CDF of the received voltage, is that of a Rayleigh distribution. The  $\text{CDF}(P_{\text{rec}}/P)$  is plotted in Fig. 5.1(a), where the reference power  $P$  is chosen as the average received power, i.e.,  $P = P_{\text{av}}$ . This CDF plot shows that, e.g., in nearly 9% of the states, the received power is at least 10 dB below the reference level  $P_{\text{av}}$ . This means that for the remaining 91% of the states, the received power is not more than 10 dB below the reference level. This means that if the threshold level  $P_{\text{th}}$  is 10 dB below the the reference level, there is 91% probability that the received power is above the threshold level. And since received power being higher than the threshold level means no error, the PoD is 91% at this level. This is also shown when the ideal threshold receiver

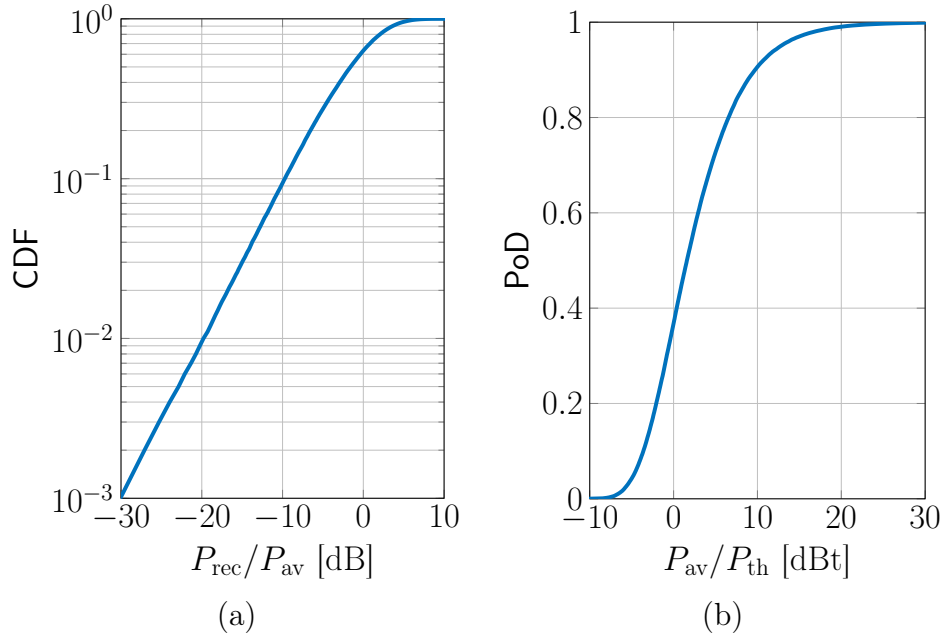


Figure 5.1: Illustration of ideal threshold receiver model for lossless isotropic antenna in RIMP (a) the CDF, and (b) the PoD.

model as described by (5.1) is used to obtain the PoD. The corresponding PoD with the above-mentioned assumptions is plotted in Fig. 5.1(b), which shows that in order to maintain an error-free link for 91% of the time, the average received power needs to be at least 10 dB above the threshold level, i.e., 10 dBt.

## 5.2 MIMO Efficiency

The power required to achieve 95% PoD level can be used as a metric for the system performance [49,50]. This value represents the power that is required at the transmitter in order for 95% of the data packets to be detected at the receiving side for a fixed coding and modulation scheme. MIMO efficiency is defined by the  $P/P_{\text{th}}$  degradation compared to an ideal antenna [50]. It is clear that a higher  $P/P_{\text{th}}$  value means that higher transmitted power is required to maintain 95% PoD level, resulting in a worse system performance. This will in turn show itself in a decreased MIMO efficiency. The MIMO efficiency can be expressed as:

$$\eta_{\text{MIMO}} = \frac{\text{PoD}_0^{-1}(0.95)}{\text{PoD}^{-1}(0.95)}, \quad (5.2)$$

where  $\text{PoD}^{-1}$  is the inverse function of  $\text{PoD}$ , and  $\text{PoD}_0$  represents the  $\text{PoD}$  of the ideal antenna as described in (5.1).

The above definition of degradation at the 95%  $\text{PoD}$  level corresponds to the MIMO efficiencies defined in [50, 51] for RIMP environments. The difference between RIMP and Random-LOS is the choice of the reference antenna as described earlier. In RIMP the ideal antenna is chosen as a lossless isotropic antenna, while in Random-LOS a lossless coverage and polarization matched antenna is chosen. Here, polarization-matched means that regardless of the random polarization of the incoming plane wave, all its power is received by the antenna and no part is missed due to polarization mismatch. Coverage-matched means that the radiation pattern of the ideal antenna should cover the whole intended coverage area of the AUT with uniform directive gain.

In the present thesis, we use the MIMO efficiency to characterize the antenna for both the 1-bitstream (diversity) and 2-bitstream (MIMO) systems. When the MIMO efficiency is evaluated for a 1-bitstream diversity system, it corresponds in reality to a SIMO (receive diversity) efficiency. However, to avoid confusion of the terms, we use MIMO efficiency as a general term covering all cases. The 1- and 2-bitstream systems, The MIMO algorithms and related concepts are detailed in Chapter 6.

In Random-LOS, the MIMO efficiency can be calculated for any given antenna at any AoA, assuming random polarization. We can even readily extend the definition to a given range of AoAs, i.e., a given bitstream coverage, to get the MIMO efficiency as a function of AoA [52]. This definition is used in the attached papers to plot the bitstream coverage for different antennas using different MIMO algorithms.

For 1-bitstream systems, it is also possible to define the efficiency based on the degradation in the diversity gain at the 5% level. However, it can be shown that such definition will yield the exact same efficiency values as the definition based on the  $\text{PoD}$ . It should be mentioned that the diversity gain in RIMP is often defined at the 1% CDF level [53, 54]. Instead, here we choose a definition at the 5% CDF level (corresponding to 95%  $\text{PoD}$  level) because in practical situations this can be determined much more accurately than at the 99%  $\text{PoD}$  level. In addition, 95% is often used as the reference for the throughput performance, see, e.g., [49].

In 2-bitstream systems, each of the separate bitstreams has its own  $\text{PoD}$  curve. The  $\text{PoDs}$  of the two bitstreams are not necessarily equal. The MIMO efficiency of a 2-bitstream system is defined based on the worse performing bitstream, i.e., the one with lower received power. The reason for this choice is that it is the worst channel that becomes the bottleneck, limiting the system performance in practice.

# Chapter 6

## Multi-Antenna Systems

Multiple antenna elements have traditionally been used as antenna arrays, which have been used widely in, e.g., radar systems, satellite communications, and mobile communication systems at the base-station side. Antenna arrays provide flexibility in terms of beam-width, beam steering and gain. As another example, a large aperture is needed to obtain high directivity, which can be achieved by using an antenna array. However, in these examples, the antenna array is still treated as a single antenna with a single radiation pattern and port.

The system performance in a fading environment can be improved by using individual antenna ports and post-processing the signals at several of them. In order for the diversity or multiplexing techniques to work well, the signals at the individual antenna ports have to be sufficiently uncorrelated.

### 6.1 Diversity

In multipath, the transmitted signal reaches the receiver antenna through two or more paths. Hence, the received signal is comprised of the combination of multiple copies of the transmitted signal which have propagated through different paths and thus have undergone different attenuations, phase shifts and polarization shifts. Depending on the phase differences, these different contributions can add up in constructive or destructive ways, which leads to the fading of the received signal. In Random-LOS the fading is caused by the random orientation of the antenna, random positions of the users, or both. The incoming wave can be incident on a null in the antenna's radiation pattern or can have a polarization mismatch with the receiver antenna.

In both cases using two or more receiver antennas can help reduce the effect of the fading. If the signals at the individual antenna ports are suffi-

ciently uncorrelated, it is unlikely that the signal level is low at all ports at the same time. The individual signals can then be combined in an optimal way to extract the transmitted signal. This technique is called diversity. Diversity can be achieved by different means, e.g., frequency, spatial, or polarization diversity. To use spatial diversity in LOS, the separation between the antennas needs to be very large in terms of wavelength [55], which makes it impractical. Instead, since the polarization in Random-LOS is random, polarization diversity can be employed. It should be noted that in a Random-LOS channel we can have maximum two independent polarizations.

Different combining methods are available, most of which are linear, i.e., the output of the combiner is the weighted sum of the signals at the different antenna ports [56]. The weights can be binary (only one weight is one at any given time and all the others are zero), such as in Selection Combining (SC) or Switch and Stay Combining (SSC). All the weights can also be non-zero as in Maximal Ratio Combining (MRC) and Equal-Gain Combining (EGC). Of these combining methods, MRC is the most frequently used in the current work. In MRC the weights are chosen proportionally to the SNR at the ports. It can be shown that the combined SNR in a MRC system is equal to [56]

$$\gamma_{\text{MRC}} = \sum_{i=1}^{N_r} \gamma_i, \quad (6.1)$$

where  $N_r$  is the number of individual ports and  $\gamma_i$  is the SNR of the  $i$ -th port.

## 6.2 MIMO

A system where both the transmitter and the receiver sides have multiple antennas is referred to as multiple-input multiple-output (MIMO). In MIMO systems, the structure of the channel matrix is exploited to obtain independent signal paths between the transmitter and receiver ends, in order to increase the data rate or improve the performance [56]. The data stream to be transmitted is demultiplexed into two or more sub-streams and is transmitted simultaneously from the transmitter antennas. The transmitter can then differentiate between the multiple streams and process them to yield the original stream [57]. The input-output relation can thus be written as [58]

$$\mathbf{y} = \mathbf{H}\mathbf{x} + \mathbf{n}, \quad (6.2)$$

where  $\mathbf{y} \in \mathbb{C}^{N_r \times 1}$  denotes a vector of the received signals,  $\mathbf{x} \in \mathbb{C}^{N_t \times 1}$  is a vector containing the transmitted signals,  $\mathbf{H} \in \mathbb{C}^{N_r \times N_t}$  is the MIMO channel

matrix, and  $\mathbf{n} \in \mathbb{C}^{N_r \times 1}$  is the noise vector containing independent identically distributed (i.i.d.) unit variance Gaussian-distributed elements.  $N_r$  and  $N_t$  denote the number of receive and transmit antennas, respectively. The elements of the channel matrix  $\mathbf{H}$  are proportional to the induced voltages at the ports of the receiver antenna. The number of maximum parallel data streams that can be obtained is given by  $\min\{N_r, N_t\}$ . Since in a Random-LOS channel we can have maximum two independent polarizations, the polarization MIMO system in Random-LOS can support maximum two data streams.

Depending on the availability of the Channel State Information (CSI) at receiver and transmitter sides, different schemes have been proposed to extract the data. Two techniques that are frequently used in the current work are Zero Forcing (ZF) and Singular Value Decomposition (SVD), both of which require the CSI. ZF relies on the pseudo-inversing of the channel matrix  $\mathbf{H}$ , while SVD exploits the singular value decomposition of the channel matrix, as suggested by the name.

In ZF, the SNR of the  $i$ -th data stream is obtained as [57]

$$\gamma_i^{\text{ZF}} = \frac{\gamma_t}{N_t \left[ (\mathbf{H}^H \mathbf{H})^{-1} \right]_{i,i}}, \quad (6.3)$$

where,  $\gamma_t$  is the transmit SNR and  $[\mathbf{X}]_{i,i}$  the  $i$ -th diagonal element of the matrix  $\mathbf{X}$  for  $i = \{1, 2\}$ .  $\mathbf{X}^{-1}$  and  $\mathbf{X}^H$  denote the matrix inversion operation and Hermitian transpose, respectively.

Different power allocation schemes can be used for SVD. That means transmitter can allocate different power to different bitstreams, based on the CSI. For example, the water-filling scheme uses more power on the bitstream which has better SNR, while in inverse power allocation [59] higher power is allocated to the bitstream with lower SNR. The SNR of the data streams in SVD with equal power allocation are obtained as [56]

$$\gamma_i^{\text{SVD}} = \frac{\lambda_i \gamma_t}{N_t}, \quad (6.4)$$

where  $\lambda_i$  are the eigenvalues of  $\mathbf{H}^H \mathbf{H}$ .

In ZF there is no need for CSI at the transmitter side, whereas this is not the case for SVD. The CSI is needed at the SVD transmitter to adjust the power allocation. The performance of the SVD algorithm depends on the power allocation scheme. It has been shown that SVD inverse power allocation leads to better PoD compared to ZF and equal power SVD in RIMP [59].

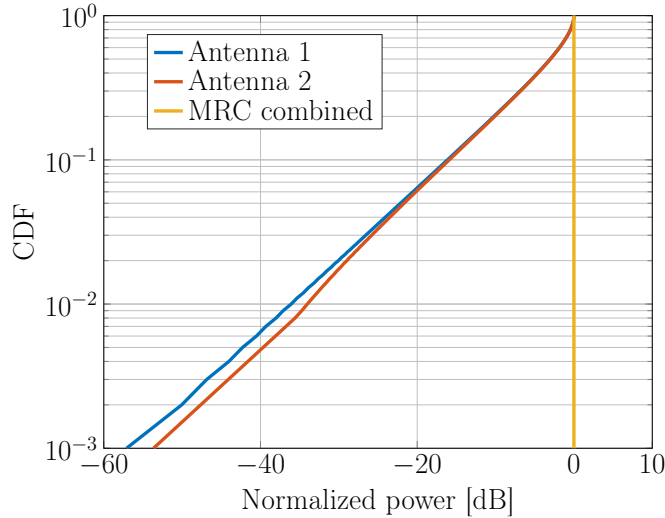


Figure 6.1: The CDF of the received power at the two antenna ports and the MRC combined power, subject to an incoming plane wave with random polarization. The two antennas are assumed to have orthogonal and equal-amplitude far-field functions.

### 6.3 Polarization-diversity and Polarization-MIMO Antennas

Dual-polarized antennas are used for  $2 \times 1$  diversity or  $2 \times 2$  MIMO systems in Random-LOS. If the far-field functions of the receiver antennas are orthogonal and equal-amplitude, the transmitted signal can be recovered regardless of polarization mismatch, by using MIMO algorithms [4, Sec. 3.10]. Fig. 6.1 shows the CDF of the signal at each antenna port and after applying MRC for such a case in a  $2 \times 1$  system. It is observed that while the signal at each port undergoes fading due to the random polarization mismatch, the envelope of the combined signal is independent of the polarization. However, when the far-fields are not orthogonal or not equal-amplitude, the MRC algorithm is no longer able to recover the power completely.

Small orthogonal antennas have very often far-fields that are orthogonal and balanced only in one specific main direction. This is in particular the case for orthogonal dipole and patch antennas. If the antenna has two symmetry planes, the far-fields of the two ports will also be orthogonal in the symmetry planes, but they may not be amplitude-balanced there. Between the symmetry planes there can also be significant cross-polar field levels (see, e.g., the BOR<sub>1</sub> antenna relations in [4, Sec. 2.4.2]). These deficiencies will

### 6.3. POLARIZATION-DIVERSITY AND POLARIZATION-MIMO ANTENNAS

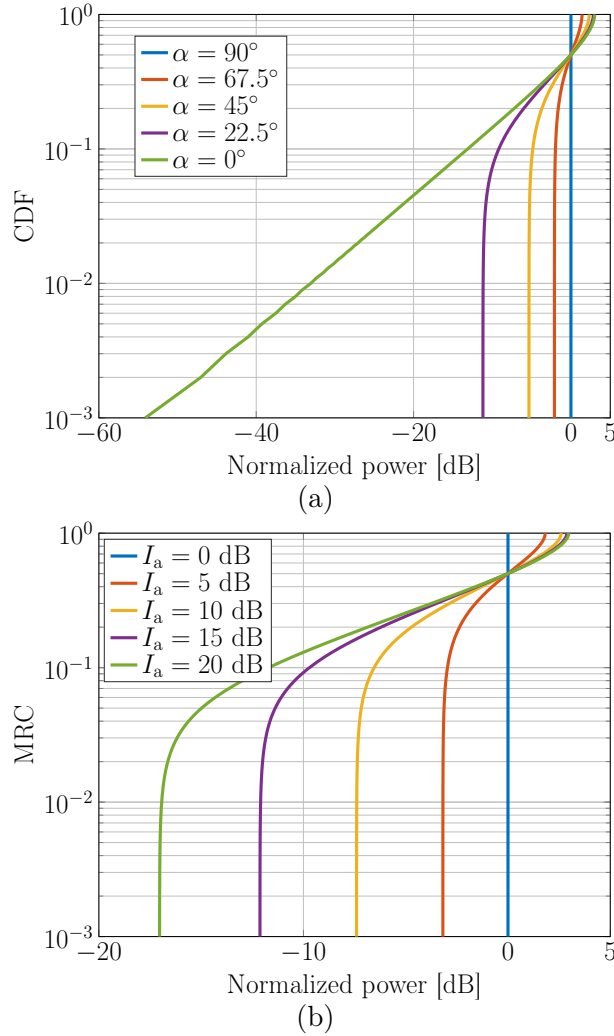


Figure 6.2: The CDF of the MRC combined power, when two antennas are subject to an incoming plane wave with random polarization. The far-field vectors are (a) equal-amplitude but make an angle  $\alpha$ , and (b) orthogonal but the amplitude of one is  $I_a$  dB larger than the other.

affect the system performance in a Random-LOS environment, in a different way than in fixed LOS-dominated polarization multiplexing systems. For those AoAs where the far-fields of the two antenna ports are non-orthogonal or amplitude-balanced, the MIMO algorithms can not fully compensate the random polarization mismatch. Fig. 6.2(a) shows the combined power when the two far-field vectors are equal but form different angles, while Fig. 6.2(b) shows the case where the far-fields are orthogonal, but have different amplitudes.

In order to investigate the effects of these polarization deficiencies, we

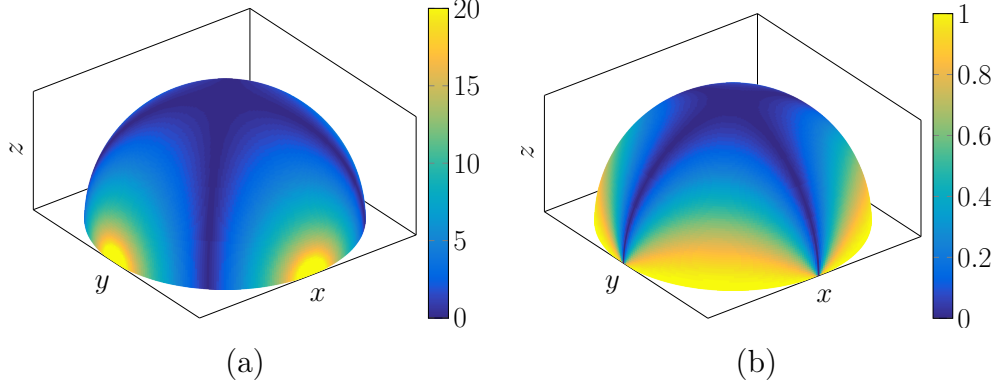


Figure 6.3: (a)  $I_a$ , amplitude imbalance in dB, and (b)  $I_p$ , polarization non-orthogonality, of two orthogonal half-wave dipoles oriented along the  $x$ - and  $y$ -axes, respectively.

characterize the far-field functions of dual-polarized antennas by defining two parameters, namely *polarization non-orthogonality* and *amplitude imbalance*. Let us assume that the far-field functions of the two receiving antennas are defined as  $\mathbf{G}_1(\theta, \phi)$  and  $\mathbf{G}_2(\theta, \phi)$  at any direction  $(\theta, \phi)$  in space. Then, the amplitude imbalance is defined for any direction as

$$I_a(\theta, \phi) = \frac{\max\{|\mathbf{G}_1|, |\mathbf{G}_2|\}}{\min\{|\mathbf{G}_1|, |\mathbf{G}_2|\}}, \quad (6.5)$$

which is the ratio of the amplitudes of the two far-field functions,  $0 \leq I_a(\theta, \phi) \leq 1$ . Furthermore, we define the polarization non-orthogonality as

$$I_p(\theta, \phi) = \frac{|\mathbf{G}_1 \cdot \mathbf{G}_2^*|}{|\mathbf{G}_1| |\mathbf{G}_2|}. \quad (6.6)$$

The far-field functions are desired to be as close to orthogonal as possible, hence when  $\mathbf{G}_1$  and  $\mathbf{G}_2$  are orthogonal, we have  $I_p = 0$ .  $I_p$  reaches its maximum when the two far-field vectors are parallel and  $0 \leq I_p(\theta, \phi) \leq 1$ .

The polarization non-orthogonality and amplitude imbalance may both be pronounced (i.e.,  $I_a$  and  $I_p$  closer to 1 rather than 0) at most AoAs, even if the antenna elements (ports) themselves are orthogonal, i.e., uncoupled. The presence of these polarization deficiencies and their spatial extent is best understood by and example. We consider two co-located orthogonally polarized half-wavelength dipoles, located at the origin of the coordinate system. The dipoles are assumed to be  $x$ - and  $y$ -polarized, respectively. Knowing the far-field function of the half-wave dipole,  $I_a$  and  $I_p$  can be determined for every  $\theta$  and  $\phi$  angle. Fig. 6.3 shows the spatial distribution of  $I_p$  and  $I_a$  in dB in this combination, in the half-space above the  $xy$ -plane.

### 6.3. POLARIZATION-DIVERSITY AND POLARIZATION-MIMO ANTENNAS

It is observed that except for the boresight direction, the orthogonal receiving antenna ports are not providing orthogonal polarizations with equal amplitude. These deficiencies are not limited to dipole antennas and similar imbalances may also appear away from broadside for other orthogonal antennas.

The effects of the aforementioned polarization deficiencies on the performance of polarization-MIMO systems are numerically studied in Paper 4. Furthermore, Paper 5 provides an analytical approach to obtain the PoD curves of dual-polarized antennas in the presence of the polarization deficiencies in general. Paper 6, covers the Random-LOS MIMO performance characterization of a planar Eleven antenna that is designed for use as a micro base-station antenna. It is shown that the polarization deficiencies will degrade the MIMO efficiency.



# Chapter 7

## Summary of the Included Papers and Future Research Directions

A brief summary of the papers that are included in the thesis, is provided in this chapter. Full versions of the papers are available in Part II. The papers have been reformatted in order to comply with the rest of the thesis.

### **Paper 1: Optimal Size of Uniform Aperture for Near-field Penetration Through Lossy Medium**

Axial pattern, or the intensity of the radiated field along the axis of an aperture, has traditionally been used to characterize the focus of antennas in the near-field. However, this does not efficiently characterize the near-field focus in lossy media. In this paper, we have introduced the 3dB near-field beam radius to characterize the focus in the presence of loss. The 3dB beam radius is then used to estimate the optimal size of uniform field apertures for near-field sensing applications, in order to maximize the detection probability of foreign objects in homogeneous lossy media with a through sensing system. We have investigated the effects of the size of the aperture and the loss tangent of the medium on the focusing properties of the apertures. The effect of a correctly chosen aperture size on the scattered power from foreign objects in the lossy medium has also been demonstrated.

### **Paper 2: Maximum Aperture Power Transmission in Lossy Homogeneous Matters**

In this paper, a generic numerical method is presented for determining the optimal aperture field distribution that maximizes the near-field power transfer through lossy media between two apertures. The effects of the size of the apertures as well as the spacing between the two are investigated, and

the fundamental limitations on power transfer in lossy medium are studied. The numerical method is easy to implement and can be applied to apertures of different geometries. It can also be used to determine the upper bound of near-field power transfer in the presence of conductive loss.

### **Paper 3: Optimal Aperture Distribution for Maximum Power Transfer in Planar Lossy Multilayered Matters**

Although the formulation in Paper 2 was originally derived for homogeneous media, it can be easily extended to any non-homogeneous media as long as the Green's function of the emanated fields from the basis functions are known. Numerical tools are used in this paper to obtain the Green's function in planar multi-layered lossy media in the spectral domain. The Green's function is then used to determine the optimal aperture distributions to maximize the near-field power through the structure. The optimal aperture distribution is determined in the absence of any foreign objects, but we have formulated a MoM approach in the spectral domain to calculate the scattered field from a PEC patch located in the media between the two apertures. It is shown that the optimal aperture distribution increases the detection probability of the foreign object.

### **Paper 4: Characterizing Polarization-MIMO Antennas in Random-LOS Propagation Channels**

In this paper, a numerical study on the performance of dual-polarized antennas in Random-LOS is presented. In order to employ spatial diversity in LOS, the spacing between the diversity antennas needs to be very large which makes it impractical. Instead, polarization diversity can be used in Random-LOS. Ideally, the antenna far-fields should be orthogonal and have equal amplitudes for polarization diversity in LOS. However, dual-polarized antennas do not provide orthogonal and amplitude-balanced far-field pattern vectors at every direction. This leads to performance degradations when these antennas are used in polarization-diversity or polarization-MIMO systems in Random-LOS. We have introduced two types of deficiencies for dual-polarized antennas in Random-LOS and studied the effect of these deficiencies on the system performance.

### **Paper 5: Probability of Detection Functions of Polarization-MIMO Systems in Random-LOS**

In this paper, we have provided analytical formulas to obtain the 1-bitstream MRC and 2-bitstream ZF PoD curves for dual-polarized antennas in Random-LOS. The PoD was numerically computed in Paper 4 through simulations of many cases. These closed-form formulas provides a better

insight into the system performance, without the need to run potentially complex and time-consuming simulations. The effects of the polarization deficiencies on the MIMO efficiency are studied analytically and the formulas are applied to a dual-polarized self-grounded bowtie antenna in order to study its performance in Random-LOS.

### **Paper 6: Design of a Planar Eleven Antenna for Optimal Probability of Detection as a Wideband MIMO Micro-base Station Antenna**

In this paper, a novel planar Eleven antenna is presented as a dual-polarized micro base-station antenna for the 1.6–2.8 GHz frequency band. It is possible to use the presented antenna in 2-, 4-, and 8-port modes. The performance of the antenna in both RIMP and Random-LOS environments is investigated and presented. The antenna design is carried out having the Random-LOS performance in mind. As a result, the antenna shows good MIMO efficiency in Random-LOS, with small variations over the frequency band of operation.

### **Paper 7: Characterization Method of an Automotive Random-LOS OTA Measurement Setup**

A chamber antenna for automotive Random-LOS OTA measurements is proposed and studied in this paper. A semi-anechoic chamber (with reflecting ground plane) is used for automotive measurements, and an array-fed reflector antenna is proposed as the chamber antenna. Due to size constraints, the car will be located in the near-field of the chamber antenna. The objective is to have a homogeneous field distribution over a test zone, where the antenna under test (AUT) will be located. A homogeneous field distribution will contribute to lower uncertainty in the measurements. The effects of the ground plane and the tilting of the chamber antenna are studied. Furthermore, the effects of both direct radiation from the feed and the radiated field from the reflector on the variations of the field in the test zone are studied. It is shown that the direct radiation into the test zone has a negative effect on the homogeneity of the field distribution and the accuracy of the measurements.

### **Paper 8: Back-of-the-envelope Evaluation of the Prevalence of RIMP or LOS Propagation as a Function of Frequency**

As the operating frequency of wireless communication systems increases, the multipath effects are expected to decrease and the Random-LOS propagation scenario to become the more prevalent one. Due to the complica-

tions in the modeling of specific large-scale scattering environments, we have chosen a statistical approach with generic scattering environments where a number of resonant scatterers are distributed randomly in space. In this paper, we have presented a back-of-the-envelope study of the frequency-dependence of the RIMP and Random-LOS propagation scenarios in such generic scattering environment, in order to demonstrate the aforementioned effect. A simple analytical model and full-wave MoM simulations are used to facilitate the study, where a good agreement between the two is observed.

## 7.1 Future Research Directions

Following the work presented in this thesis there are still challenges to face and possible extensions can be made. Accordingly, the research activity can be continued in the following directions:

- The method used in Papers 2 and 3 to determine the optimal aperture distribution can be extended to apertures of different shapes and forms, as well as different media combinations in specific applications.
- Papers 2 and 3 explore some of the fundamental limits of power transfer in lossy media. However, the final objective in this process is to actually generate an aperture field that is as close as possible to the optimal one for a specific application. Hence, an interesting extension of this work is to design and manufacture antennas for different near-field applications.
- Further studies can be aimed at thoroughly verifying the real-life hypothesis presented in Chapter 4.
- Guidelines are developed for the requirements of dual-polarized antennas for Random-LOS in Papers 4 and 5, and an antenna designed with Random-LOS performance in mind is presented in Paper 6. An interesting research direction will be on the design of new antennas for Random-LOS, especially large array antennas for massive MIMO.
- The Random-LOS automotive measurement setup in Paper 7 remains to be manufactured and its accuracy needs to be verified. In general, the research on OTA measurement tools and procedures for Random-LOS are ongoing and further work needs to be done in this respect.

# References

- [1] S. Hong, *Wireless: From Marconi's Black-Box to the Audion*. MIT Press, 2010.
- [2] "IEEE standard for definitions of terms for antennas," *IEEE Std 145-2013 (Revision of IEEE Std 145-1993)*, pp. 1–50, March 2014.
- [3] C. A. Balanis, *Antenna Theory: Analysis and Design*. John Wiley and Sons, 2005.
- [4] P.-S. Kildal, *Foundations of Antennas: A Unified Approach for Line-of-Sight and Multipath*. Kildal Antenn AB, 2015, Available at [www.kildal.se](http://www.kildal.se).
- [5] R. Marhefka and D. Kraus, *Antennas for All Applications*. McGraw-Hill, 2002.
- [6] K. Rosengren and P.-S. Kildal, "Radiation efficiency, correlation, diversity gain and capacity of a six-monopole antenna array for a MIMO system: theory, simulation and measurement in reverberation chamber," *IEE Proceedings - Microwaves, Antennas and Propagation*, vol. 152, no. 1, pp. 7–16, 2005.
- [7] X. Li, E. Bond, B. Van Veen, and S. Hagness, "An overview of ultra-wideband microwave imaging via space-time beamforming for early-stage breast-cancer detection," *IEEE Antennas and Propagation Magazine*, vol. 47, no. 1, pp. 19–34, 2005.
- [8] Y. Yu, J. Yang, T. McKelvey, and B. Stoew, "A compact UWB indoor and through-wall radar with precise ranging and tracking," *International Journal of Antennas and Propagation*, 2012.
- [9] S. Fayazi, J. Yang, and H. Lui, "UWB SAR imaging of near-field object for industrial process applications," in *Proceedings of the 7th European Conference on Antennas and Propagation (EuCAP 2013)*, Gothenburg, Sweden, April 2013.

## REFERENCES

- [10] X. Zeng, A. Fhager, P. Linner, M. Persson, and H. Zirath, "Experimental investigation of the accuracy of an ultrawideband time-domain microwave-tomographic system," *IEEE Transactions on Instrumentation and Measurement*, vol. 60, no. 12, pp. 3939–3949, 2011.
- [11] K. Sanghoek, J. Ho, and A. Poon, "Wireless power transfer to miniature implants: Transmitter optimization," *IEEE Transactions on Antennas and Propagation*, vol. 60, no. 10, pp. 4838–4845, 2012.
- [12] A. Razavi and J. Yang, "Investigation of penetration ability of UWB antennas in near-field sensing applications," in *Proceedings of the 6th European Conference on Antennas and Propagation (EuCAP 2012)*, Prague, Czech Republic, March 2012.
- [13] D. C. Cox, "Antenna diversity performance in mitigating the effects of portable radiotelephone orientation and multipath propagation," *IEEE Transactions on Communications*, vol. 31, no. 5, pp. 620–628, 1983.
- [14] W. Fan, X. Carreno, P. Kyosti, J. O. Nielsen, and G. F. Pedersen, "Over-The-Air testing of MIMO-capable terminals: Evaluation of multiple-antenna systems in realistic multipath propagation environments using an OTA method," *IEEE Vehicular Technology Magazine*, vol. 10, no. 2, pp. 38–46, June 2015.
- [15] A. A. Glazunov, V.-M. Kolmonen, and T. Laitinen, "MIMO over-the-air testing," *LTE-Advanced and Next Generation Wireless Networks: Channel Modelling and Propagation*, pp. 411–441, 2012.
- [16] P.-S. Kildal, C. Orlenius, and J. Carlsson, "OTA testing in multipath of antennas and wireless devices with MIMO and OFDM," *Proceedings of the IEEE*, vol. 100, no. 7, pp. 2145–2157, 2012.
- [17] M. G. Nilsson, P. Hallbjörner, N. Arabäck, B. Bergqvist, T. Abbas, and F. Tufvesson, "Measurement uncertainty, channel simulation, and disturbance characterization of an over-the-air multiprobe setup for cars at 5.9 GHz," *IEEE Transactions on Industrial Electronics*, vol. 62, no. 12, pp. 7859–7869, 2015.
- [18] P.-S. Kildal, "Rethinking the wireless channel for OTA testing and network optimization by including user statistics: RIMP, pure-LOS, throughput and detection probability," in *Proceedings of the 2013 International Symposium on Antennas and Propagation (ISAP)*, Nanjing, China, October 2013.

- [19] P. H. Lehne, K. Mahmood, A. A. Glazunov, P. Gronsund, and P.-S. Kildal, "Measuring user-induced randomness to evaluate smart phone performance in real environments," in *Proceedings of the 9th European Conference on Antennas and Propagation (EuCAP 2015)*, Lisbon, Portugal, April 2015.
- [20] S. A. Bergmann and H. W. Arnold, "Polarisation diversity in portable communications environment," *Electronics Letters*, vol. 22, no. 11, pp. 609–610, 1986.
- [21] J. W. Sherman, "Properties of focused apertures in the Fresnel region," *IRE Transactions on Antennas and Propagation*, vol. 10, no. 31, pp. 399–408, July 1962.
- [22] R. C. Hansen, "Focal region characteristics of focused array antennas," *IEEE Transactions on Antennas and Propagation*, vol. 33, no. 12, pp. 1328–1337, December 1985.
- [23] W. J. Graham, "Analysis and synthesis of axial field patterns of focused apertures," *IEEE Transactions on Antennas and Propagation*, vol. 31, no. 4, pp. 665–668, July 1983.
- [24] S. Karimkashi and A. Kishk, "Focused microstrip array antenna using a Dolph-Chebyshev near-field design," *IEEE Transactions on Antennas and Propagation*, vol. 57, no. 12, pp. 3813–3820, December 2009.
- [25] —, "Focusing properties of Fresnel zone plate lens antennas in the near-field region," *IEEE Transactions on Antennas and Propagation*, vol. 59, no. 5, pp. 1481–1487, May 2011.
- [26] G. Schmid, G. Neubauer, and P. Mazal, "Dielectric properties of human brain tissue measured less than 10 h postmortem at frequencies from 800 to 2450 MHz," *Bioelectromagnetics*, vol. 24, no. 6, pp. 423–430, 2003.
- [27] C. A. Balanis, *Advanced Engineering Electromagnetics*. John Wiley and Sons, 1989.
- [28] A. Razavi, R. Maaskant, J. Yang, and M. Viberg, "Optimal aperture distribution for near-field detection of foreign objects in lossy media," in *Proceedings of the IEEE-APS Topical Conference on Antennas and Propagation in Wireless Communications (IEEE APWC '14)*. Palm beach, Aruba: IEEE, August 2014.

## REFERENCES

- [29] A. Razavi, R. Maaskant, J. Yang, Z. Šipuš, and M. Viberg, “Optimal aperture distribution for maximum power transfer in planar lossy multilayered matters,” in *Proceedings of the 9th European Conference on Antennas and Propagation (EuCAP 2015)*, Lisbon, Portugal, April 2015.
- [30] A. F. Kay, “Near-field gain of aperture antennas,” *IRE Transactions on Antennas and Propagation*, vol. 8, no. 6, pp. 586–593, November 1960.
- [31] G. V. Borgiotti, “Maximum power transfer between two planar apertures in the Fresnel zone,” *IEEE Transactions on Antennas and Propagation*, vol. 14, no. 2, pp. 158–163, March 1966.
- [32] S. Gabriel, R. Lau, and C. Gabriel, “The dielectric properties of biological tissues: III. Parametric models for the dielectric spectrum of tissues,” *Physics in medicine and biology*, vol. 41, 1996.
- [33] Z. Šipuš, P.-S. Kildal, R. Leijon, and M. Johansson, “An algorithm for calculating Green’s functions of planar, circular cylindrical, and spherical multilayer substrates,” *Applied Computational Electromagnetics Society (ACES) Journal*, no. 3, pp. 243–254, 1998.
- [34] K. Rosengren, P.-S. Kildal, C. Carlsson, and J. Carlsson, “Characterization of antennas for mobile and wireless terminals in reverberation chambers: Improved accuracy by platform stirring,” *Microwave and Optical Technology Letters*, vol. 30, no. 6, pp. 391–397, 2001.
- [35] J. G. Kostas and B. Boverie, “Statistical model for a mode-stirred chamber,” *IEEE Transactions on Electromagnetic Compatibility*, vol. 33, no. 4, pp. 366–370, 1991.
- [36] C. L. Holloway, D. A. Hill, J. M. Ladbury, P. F. Wilson, G. Koepke, and J. Coder, “On the use of reverberation chambers to simulate a Rician radio environment for the testing of wireless devices,” *IEEE Transactions on Antennas and Propagation*, vol. 54, no. 11, pp. 3167–3177, 2006.
- [37] C. Lemoine, E. Amador, and P. Besnier, “On the K-factor estimation for Rician channel simulated in reverberation chamber,” *IEEE Transactions on Antennas and Propagation*, vol. 59, no. 3, pp. 1003–1012, 2011.
- [38] X. Chen, P.-S. Kildal, and S.-H. Lai, “Estimation of average Rician K-factor and average mode bandwidth in loaded reverberation chamber,”

- IEEE Antennas and Wireless Propagation Letters*, vol. 10, pp. 1437–1440, 2011.
- [39] O. Delangre, P. D. Doncker, M. Lienard, and P. Degauque, “Delay spread and coherence bandwidth in reverberation chamber,” *Electronics letters*, vol. 44, no. 5, pp. 328–329, 2008.
- [40] X. Chen, P.-S. Kildal, C. Orlenius, and J. Carlsson, “Channel sounding of loaded reverberation chamber for over-the-air testing of wireless devices: Coherence bandwidth versus average mode bandwidth and delay spread,” *IEEE Antennas and Wireless Propagation Letters*, vol. 8, pp. 678–681, 2009.
- [41] K. Karlsson, X. Chen, P.-S. Kildal, and J. Carlsson, “Doppler spread in reverberation chamber predicted from measurements during step-wise stationary stirring,” *IEEE Antennas and Wireless Propagation Letters*, vol. 9, pp. 497–500, 2010.
- [42] X. Chen, P.-S. Kildal, and J. Carlsson, “Determination of maximum Doppler shift in reverberation chamber using level crossing rate,” in *Proceedings of the 5th European Conference on Antennas and Propagation (EuCAP 2011)*, Rome, Italy, April 2011.
- [43] P. Kildal and J. Carlsson, “New approach to OTA testing: RIMP and pure-LOS reference environments & a hypothesis,” in *Proceedings of the 7th European Conference on Antennas and Propagation (EuCAP 2013)*, Gothenburg, Sweden, April 2013, pp. 315–318.
- [44] M. S. Kildal, J. Kvarnstrand, J. Carlsson, A. Majidzadeh, P.-S. Kildal *et al.*, “Initial measured OTA throughput of 4G LTE communication to cars with roof-mounted antennas in 2D Random-LOS,” in *Proceedings of the 2015 International Symposium on Antennas and Propagation (ISAP)*, Hobart, Australia, November 2015.
- [45] M. S. Kildal, J. Carlsson, J. Kvarnstrand, A. Majidzadeh, P.-S. Kildal *et al.*, “Measured probabilities of detection for 1-and 2 bitstreams of 2-port car-roof antenna in RIMP and Random-LOS,” in *Proceedings of the 10th European Conference on Antennas and Propagation (EuCAP 2016)*, Davos, Switzerland, April 2016.
- [46] X. Gao, O. Edfors, F. Rusek, and F. Tufvesson, “Massive MIMO performance evaluation based on measured propagation data,” *IEEE Transactions on Wireless Communications*, vol. 14, no. 7, pp. 3899–3911, 2015.

## REFERENCES

- [47] H. Q. Ngo, E. G. Larsson, and T. L. Marzetta, “Aspects of favorable propagation in massive MIMO,” in *Proceedings of the 22nd European Signal Processing Conference (EUSIPCO 2014)*, Lisbon, Portugal, September 2014, pp. 76–80.
- [48] P.-S. Kildal, A. Hussain, X. Chen, C. Orlenius, A. Skårbratt, J. Åsberg, T. Svensson, and T. Eriksson, “Threshold receiver model for throughput of wireless devices with MIMO and frequency diversity measured in reverberation chamber,” *IEEE Antennas and Wireless Propagation Letters*, vol. 10, pp. 1201–1204, 2011.
- [49] A. Hussain, P.-S. Kildal, and A. A. Glazunov, “Interpreting the total isotropic sensitivity and diversity gain of LTE-enabled wireless devices from over-the-air throughput measurements in reverberation chambers,” *IEEE Access*, vol. 3, pp. 131–145, 2015.
- [50] X. Chen, “Throughput modeling and measurement in an isotropic-scattering reverberation chamber,” *IEEE Transactions on Antennas and Propagation*, vol. 62, no. 4, pp. 2130–2139, 2014.
- [51] X. Chen, P.-S. Kildal, and M. Gustafsson, “Characterization of implemented algorithm for MIMO spatial multiplexing in reverberation chamber,” *IEEE Transactions on Antennas and Propagation*, vol. 61, no. 8, pp. 4400–4404, 2013.
- [52] S. M. Moghaddam, A. A. Glazunov, J. Yang, M. Gustafsson, and P.-S. Kildal, “Comparison of 2-bitstream polarization-MIMO performance of 2 and 4-port bowtie antennas for LTE in random-LOS,” in *Proceedings of the 2015 International Symposium on Antennas and Propagation (ISAP)*, Hobart, Australia, November 2015.
- [53] P.-S. Kildal, K. Rosengren, J. Byun, and J. Lee, “Definition of effective diversity gain and how to measure it in a reverberation chamber,” *Microwave and Optical Technology Letters.*, vol. 34, no. 1, pp. 56–59, 2002.
- [54] N. Jamaly, P.-S. Kildal, and J. Carlsson, “Compact formulas for diversity gain of two-port antennas,” *IEEE Antennas and Wireless Propagation Letters*, vol. 9, pp. 970–973, 2010.
- [55] T. Ingason and H. Liu, “Line-of-sight MIMO for microwave links-adaptive dual polarized and spatially separated systems,” Master’s thesis, Chalmers University of Technology, Sweden, 2009.

- [56] A. Goldsmith, *Wireless Communications*. Cambridge University Press, 2005.
- [57] A. Paulraj, R. Nabar, and D. Gore, *Introduction to Space-Time Wireless Communications*. Cambridge University Press, 2003.
- [58] E. Telatar, “Capacity of multi-antenna Gaussian channels,” *European Transactions on Telecommunications*, vol. 10, no. 6, pp. 585–595, 1999.
- [59] X. Chen, B. P. Einarsson, and P.-S. Kildal, “Improved MIMO throughput with inverse power allocation — study using USRP measurement in reverberation chamber,” *IEEE Antennas and Wireless Propagation Letters*, vol. 13, pp. 1494–1496, 2014.